Multiple phonon modes in Feynman path-integral variational polaron mobility

Bradley A. A. Martin [1] and Jarvist Moore Frost [1,2,*]

[1]*Department of Physics, Imperial College London, Exhibition Road, London SW7 2AZ, United Kingdom*

[2]*Department of Chemistry, Imperial College London, White City Campus, London W12 0BZ, United Kingdom*

(Received 30 March 2022; revised 22 December 2022; accepted 9 February 2023; published 13 March 2023)

The Feynman path-integral variational approach to the polaron problem, along with the associated Feynman-Hellwarth-Iddings-Platzman (FHIP) linear-response mobility theory, provides a computationally amenable method to predict the frequency-resolved temperature-dependent charge-carrier mobility, and other experimental observables in polar semiconductors. We show that the FHIP mobility theory predicts non-Drude transport behavior, and shows remarkably good agreement with the recent diagrammatic Monte Carlo mobility simulations of Mishchenko *et al.* [Phys. Rev. Lett. **123**, 076601 (2019)] for the abstract Fröhlich Hamiltonian. We extend this method to multiple phonon modes in the Fröhlich model action. This enables a slightly better variational solution, as inferred from the resulting energy. We carry forward this extra complexity into the mobility theory, which shows a richer structure in the frequency and temperature-dependent mobility, due to the different phonon modes activating at different energies. The method provides a computationally efficient and fully quantitative method of predicting polaron mobility and response in real materials.

DOI: 10.1103/PhysRevB.107.115203

I. INTRODUCTION

An excess electron in a polar semiconductor polarizes and distorts the surrounding lattice. This polarization then attempts to localize the electron, forming a quasiparticle state known as the polaron.

When the electron-phonon coupling is large, the extent of the polaron wave function becomes comparable to the lattice constant and a small polaron is formed where details of the interaction with the atoms are important in determining polaron properties, but the polaron itself is localized. Many studies have investigated the properties of small polarons [1–7], where many analytical and numerical studies have primarily focused on the Holstein model with a short-range electron-phonon interaction [1].

If the competition between the localizing potential and the electron kinetic energy results in a large-polaron state, larger than the unit cell, a continuum approximation is valid and the details of the interaction with the atoms can be ignored, but the polaron itself is a dynamic object. The most simple large polaron model was introduced by Fröhlich [8], of a single fermion (the electron) interacting with an infinite field of bosons (the phonon excitations of the lattice). A major simplification with regards to real materials is assuming that only one phonon mode (which is the longitudinal optical mode, of a binary material) is infrared active (thus having dielectrically mediated electron-phonon interaction) and that this mode is dispersionless. The reciprocal-space integrals then become analytic with closed form. This Fröhlich model is described by the Hamiltonian

$$\hat{H} = \frac{\mathbf{p}^2}{2m^*} + \sum_{\mathbf{k}} \hbar\,\omega_0\, a^\dagger_{\mathbf{k}} a_{\mathbf{k}} + \sum_{\mathbf{k}} (V_{\mathbf{k}}\, a_{\mathbf{k}}\, e^{i\mathbf{k}\cdot\mathbf{r}} + V^*_{\mathbf{k}}\, a^\dagger_{\mathbf{k}}\, e^{-i\mathbf{k}\cdot\mathbf{r}}). \tag{1}$$

Here $\mathbf{r}$ is the electron vector position, $\mathbf{p}$ its conjugate momentum, m^* the electron effective mass, $\hbar$ the reduced Planck constant, ω_0 the longitudinal optical phonon frequency, $a^\dagger_{\mathbf{k}}$, $a_{\mathbf{k}}$ the phonon creation and annihilation operators with phonon wave vector $\mathbf{k}$. The electron-phonon coupling parameter is

$$V_{\mathbf{k}} = i\frac{2\hbar\omega_0}{|\mathbf{k}|}\left(\sqrt{\frac{\hbar}{2m^*\omega_0}}\frac{\alpha\pi}{\Omega_0}\right)^{\frac{1}{2}}. \tag{2}$$

Here Ω_0 is the unit-cell volume, α is Fröhlich's dimensionless interaction parameter, and other variables are as above. The model is entirely characterized by the unitless parameter α.

Although this seems highly idealized, the α parameter is a direct function of the semiconductor properties: an effective mass m^* (modeling the relevant band structure of the charge carrier), a phonon frequency ω_0 (the quantization of the phonon field), and the dielectric electron-phonon coupling between them (which dominates for polar materials [9]):

$$\alpha = \frac{1}{2}\left(\frac{1}{\epsilon_{\text{optic}}} - \frac{1}{\epsilon_{\text{static}}}\right)\frac{e^2}{\hbar\omega_0}\left(\frac{2m^*\omega_0}{\hbar}\right)^{\frac{1}{2}}. \tag{3}$$

Fröhlich's Hamiltonian, though describing a simple physical system of a single effective mass electron coupled to a single-frequency phonon field, has resisted an exact solution. This is a quantum field problem, as the phonon occupation numbers can change.

One celebrated approximation is Feynman's variational path-integral approach [10]. This method is surprisingly accurate [11] considering the light computational effort, and applies for the full range of the Fröhlich α electron-phonon coupling parameter, without having to make any weak- or strong-coupling approximation. The method was extended by Feynman-Hellwarth-Iddings-Platzman [12] (commonly referred to as FHIP) to offer a prediction of temperature-dependent mobility (in the linear-response regime) for polar

*jarvist.frost@imperial.ac.uk

materials, without any empirical parameters, and without resorting to perturbation theory. This method was alternatively derived and used by Peeters and Devreese [13–16]. The textbook definition of the FHIP dc mobility is an asymptotic solution recovered from a power-series expansion of the model action around a solvable quadratic trial action. The resultant impedance function is well defined and analytic across all frequencies, temperatures, and polaron couplings (α). A generalization to finite temperatures was made by Ōsaka [17], and the addition of an external driving force by Castrigiano and Kokiantonis [18,19], and Saitoh [20].

Hellwarth and Biaggio [21] provide a method to replace the multiple phonon modes of a complex material with a single effective frequency and coupling. This approach has been used by ourselves [22–24] and others [25] to predict phenomenological properties of charge transport for direct comparison to experiment.

In this paper, we first describe the Feynman variational quasiparticle polaron approach [10], providing a consistent description with modern nomenclature and notation. We then show that the FHIP mobility theory [12] predicts non-Drude transport behavior, and agrees closely with recent diagrammatic Monte Carlo mobility predictions of Mishchenko *et al.* [26] for the abstract Fröhlich Hamiltonian.

Second, we extend the method to more accurately model complex real materials by explicitly including multiple phonon modes. Taking a multimodal generalization of the Fröhlich Hamiltonian we derive a multimodal version of the Feynman-Jensen variational expression for the free energy at all temperatures, and then follow the methodology of FHIP [12], to derive expressions for the temperature- and frequency-dependent complex impedance. Using the example of the well-characterized methylammonium lead-halide ($MAPbI_3$) perovskite semiconductor, we provide estimates of dc mobility and complex conductivity, which can now be directly measured with transient terahertz conductivity measurements [24].

A key technical discovery during this work is that direct numerical integration of the memory function $\chi(\Omega)$ of FHIP [12] (required to calculate the polaron mobility), rather than the commonly used contour-rotated integral, has more easily controlled numerical errors for frequency-dependent properties. This is significant as many previous attempts [12,21,22,27] (including ourselves), numerically evaluate the contour-rotated integral using complicated and computationally expensive power-series expansions in terms of special functions. This can be avoided entirely.

This Feynman variational method requires a relatively trivial amount of computer time, providing machine-precision answers, within the limit of the trial action, and the first-order cumulant expansion of the actions. We show good agreement with quantum Monte Carlo approaches, which can systematically approach the true solution, but at considerable computational cost; the lightweight nature of the Feynman variational approach makes it computationally tractable when extending to real materials. We therefore suggest the Feynman variational method as a generally useful approach for predicting transport properties of polar semiconductors, particularly in the computational identification of new semiconductors for renewable energy applications.

II. PATH-INTEGRAL APPROACH TO THE FRÖHLICH POLARON

A. Feynman variational approach

The 1955 Feynman variational approach [10] casts the Fröhlich polaron problem into a Lagrangian path and field integral (the *model* action), and then integrates out the infinite quantum field of phonon excitations. The result is a remapping to an effective quasiparticle Lagrangian path integral, where an electron is coupled by a nonlocal two-time Coulomb potential to another fictitious massive particle, representing the disturbance in the lattice generated by its passage at a previous time. The density matrix ρ for the electron to go from position $\mathbf{r}'$ to $\mathbf{r}''$ within an imaginary time $i\hbar\beta$ is

$$\rho(\mathbf{r}', \mathbf{r}''; \hbar\beta) = \int_{\mathbf{r}(0)=\mathbf{r}'}^{\mathbf{r}(\hbar\beta)=\mathbf{r}''} \mathcal{D}\mathbf{r}(\tau) \exp\left(-\frac{S[\mathbf{r}(\tau)]}{\hbar}\right). \quad (4)$$

The *model* action S for the Fröhlich polaron is

$$S[\mathbf{r}(\tau)] = \frac{m^*}{2}\int_0^{\hbar\beta} d\tau \left(\frac{d\mathbf{r}(\tau)}{d\tau}\right)^2 - \frac{(\hbar\omega_0)^{\frac{3}{2}}\alpha}{2\sqrt{2m^*}} \times \int_0^{\hbar\beta} d\tau \int_0^{\hbar\beta} d\sigma \, \frac{g_{\omega_0}(|\tau-\sigma|)}{|\mathbf{r}(\tau)-\mathbf{r}(\sigma)|}, \quad (5)$$

and where

$$g_{\omega_0}(\tau) = \frac{\cosh[\omega_0(\tau - \hbar\beta/2)]}{\sinh(\hbar\omega_0\beta/2)} \quad (6)$$

is the *imaginary-time* phonon correlation function.

We cannot easily evaluate the path-integral for the $1/r$ Coulomb potential, so Jensen's inequality, $\langle \exp f \rangle \geqslant \exp \langle f \rangle$, is used to approximate the effective Lagrangian by an analytically path-integrable nonlocal two-time *quadratic* Lagrangian (the *trial* action) S_0:

$$S_0[\mathbf{r}(\tau)] = \frac{m^*}{2}\int_0^{\hbar\beta} d\tau \left(\frac{d\mathbf{r}(\tau)}{d\tau}\right)^2 + \frac{C}{2}\int_0^{\hbar\beta} d\tau \times \int_0^{\hbar\beta} d\sigma \, g_{w\omega_0}(|\tau-\sigma|)[\mathbf{r}(\tau)-\mathbf{r}(\sigma)]^2. \quad (7)$$

The resulting Feynman-Jensen inequality gives a solvable upper bound to the (model) free energy

$$F \leqslant F_0 + \langle S - S_0 \rangle_0, \quad (8)$$

where F_0 is the free energy of the trial system and $\langle S - S_0 \rangle_0$ is the expectant difference in the two actions, evaluated with respect to the trial system

$$\langle S - S_0 \rangle_0 = \frac{\int \mathcal{D}\mathbf{r}(\tau)(S - S_0)e^{-S_0[\mathbf{r}]/\hbar}}{\int \mathcal{D}\mathbf{r}(\tau)e^{-S_0[\mathbf{r}]/\hbar}}. \quad (9)$$

The process is variational, in that the C (a harmonic coupling term) and w (which controls the exponential decay rate of the interaction in imaginary time) parameters are varied to minimize the right-hand side of Eq. (8), giving the lowest upper bound to the free energy. Diagrammatic Monte Carlo shows that this method approaches the true energy across a wide range of coupling parameters [11,26,28].

B. FHIP mobility

Feynman-Hellwarth-Iddings-Platzman [12] (FHIP) derive an expression for the linear response of the Fröhlich polaron to a weak, spatially uniform, time-varying electric field $\mathbf{E}(t) = E_0 \exp(i\Omega t)$, where Ω is the angular frequency of the field. The field induces a current due to the movement of the electron,

$$\mathbf{j}(\Omega) = \frac{\mathbf{E}(\Omega)}{z(\Omega)} = e\frac{d}{dt}\langle \mathbf{r}(t)\rangle, \tag{10}$$

where $z(\Omega)$ is the complex impedance function and $\langle \mathbf{r}(t)\rangle$ the expectation of the electron position. For sufficiently weak fields (in the linear-response regime), the relationship between the impedance and the Fourier transform of the Green's function $G(t)$ of the polaron is

$$\int_{-\infty}^{\infty} dt\, G(t)\, e^{-i\Omega t} = G(\Omega) = \frac{1}{\Omega z(\Omega)}, \tag{11}$$

where $G(t) = 0$ for $t < 0$.

The electric field $E(t)$ appears as an addition linear term in the Fröhlich Hamiltonian $-\mathbf{E}\cdot\mathbf{r}$. The expected electron position can be evaluated from the density matrix $\rho(t)$ of the system,

$$\langle \mathbf{r}(t)\rangle = \mathrm{Tr}\{\mathbf{r}\rho(t)\}. \tag{12}$$

Assuming that the system is initially in thermal equilibrium $\rho_0 = \exp(-\beta H)$, the time evolution of the density matrix is evaluated with

$$i\hbar\frac{\partial \rho}{\partial t} = [H, \rho]. \tag{13}$$

Therefore, the density matrix at some later time t is

$$\rho(t) = U(t)\rho_0 U'^{\dagger}(t), \tag{14}$$

where the unitary operators U and U' for time evolution are

$$U(t) = \exp\left\{-\frac{i}{\hbar}\int_0^t [H(s) - \mathbf{r}(s)\cdot\mathbf{E}(s)]ds\right\},$$
$$U'(t) = \exp\left\{-\frac{i}{\hbar}\int_0^t [H'(s) - \mathbf{r}'(s)\cdot\mathbf{E}'(s)]ds\right\}. \tag{15}$$

Here unprimed operators are time ordered with the latest times on the far left, whereas primed operators are oppositely time ordered with the latest times on the far right. [Technically, the electric field $E(t)$ is not an operator in need of time ordering, but it is useful to treat E and E' as different arbitrary functions.]

FHIP assumes that the initial state is a product state of the phonon bath and the electron system, where only the phonon oscillators are initially in thermal equilibrium $\rho_0 \propto \exp(-\hbar\beta\sum_{\mathbf{k}}\omega_{\mathbf{k}} b_{\mathbf{k}}^{\dagger} b_{\mathbf{k}})$ at temperature $T = (k_B\beta)^{-1}$. The true system would quickly thermalize to the temperature of the (much larger) phonon bath, but the linear Feynman polaron model cannot since it is entirely harmonic. As shown by Sels [29], it would be more correct to impose that the entire model system starts in thermal equilibrium. This error results in the lack of a 2β dependence in FHIP (low-temperature) dc mobility.

We can formulate $\mathrm{Tr}\{\rho(t)\}$ as a path-integral generating functional

$$\mathrm{Tr}\{\rho(t)\} \equiv \mathcal{Z}[\mathbf{E}(t), \mathbf{E}'(t)] = \int \mathcal{D}\mathbf{r}(t)\mathcal{D}\mathbf{r}'(t)\exp\left\{\frac{i}{\hbar}\Phi[\mathbf{r}(t), \mathbf{r}'(t)] + \frac{i}{\hbar}\big(S[\mathbf{r}(t), \mathbf{E}(t)] - S[\mathbf{r}'(t), \mathbf{E}'(t)]\big)\right\}, \tag{16}$$

where S is the classical action of the uncoupled electron,

$$S[\mathbf{r}(t), \mathbf{E}(t)] = \int_0^t ds\left[\frac{m^*}{2}\left(\frac{d\mathbf{r}(s)}{ds}\right)^2 + \mathbf{E}(s)\cdot\mathbf{r}(s)\right]. \tag{17}$$

$\Phi[\mathbf{r}(t), \mathbf{r}'(t)]$ is the phase of the *influence functional* [30]. The influence functional phase for the Fröhlich model $\Phi_F[\mathbf{r}(t), \mathbf{r}'(t)]$ is derived from the model action [Eq. (5)] and is given by

$$\Phi_F[\mathbf{r}(t), \mathbf{r}'(t)] = \frac{i(\hbar\omega_0)^{\frac{3}{2}}\alpha}{2\sqrt{2m^*}}\int_{-\infty}^{\infty} dt\int_{-\infty}^{\infty} ds\left[\frac{g_{\omega_0}(|t-s|)}{|\mathbf{r}(t) - \mathbf{r}(s)|} + \frac{g^*_{\omega_0}(|t-s|)}{|\mathbf{r}'(t) - \mathbf{r}'(s)|} - 2\frac{g_{\omega_0}(t-s)}{|\mathbf{r}'(t) - \mathbf{r}(s)|}\right], \tag{18}$$

where $g_{\omega_0}(t)$ is the *real-time* phonon Green's function and is given by

$$g_{\omega_0}(t) = \frac{\cos[\omega_0(t - i\hbar\beta/2)]}{\sinh(\hbar\omega_0\beta/2)}. \tag{19}$$

The double path integral is over closed paths satisfying the boundary condition $\mathbf{r}(t) - \mathbf{r}'(t) = 0$ as $t \to \pm\infty$.

The Green's function $G(t - t')$ is the response to a δ-function electric field $\mathbf{E}(s) = \boldsymbol{\epsilon}\delta(s - t) = \mathbf{E}'(s)$. It can be evaluated from the first functional derivative of the generating functional $\mathcal{Z}[\mathbf{E}(t), \mathbf{E}'(t)]$ with respect to $\mathbf{E}(t) - \mathbf{E}'(t)$. We can formulate the primed and unprimed electric fields as

$$\mathbf{E}(s) = \boldsymbol{\epsilon}\delta(s - t) + \boldsymbol{\eta}\delta(s - t'),$$
$$\mathbf{E}'(s) = \boldsymbol{\epsilon}\delta(s - t) - \boldsymbol{\eta}\delta(s - t'). \tag{20}$$

This reduces the generating *functional* $\mathcal{Z}[\mathbf{E}(t), \mathbf{E}'(t)]$ into a generating *function* $\mathcal{Z}(\boldsymbol{\epsilon}, \boldsymbol{\eta})$. The Green's function can then be evaluated from

$$G(t - t') = -\frac{\hbar^2}{2}\frac{1}{\mathcal{Z}(0,0)}\frac{\partial^2\mathcal{Z}(\boldsymbol{\epsilon}, \boldsymbol{\eta})}{\partial\boldsymbol{\epsilon}\partial\boldsymbol{\eta}}\bigg|_{\boldsymbol{\epsilon}=\boldsymbol{\eta}=0}. \tag{21}$$

In FHIP the generating function $\mathcal{Z}(\boldsymbol{\epsilon}, \boldsymbol{\eta})$ is approximated by taking the zeroth- ($\mathcal{Z}_0$) and first-order ($\mathcal{Z}_1$) terms from an expansion of the path integral around an exactly solvable harmonic system. This system is described by a quadratic influence functional phase $\Phi_0[\mathbf{r}(t), \mathbf{r}'(t)]$ that has been derived from the quadratic trial action S_0 [Eq. (7)] and is given by

$$\Phi_0[\mathbf{r}(t), \mathbf{r}'(t)] = -\frac{iC}{2}\int_{-\infty}^{\infty} dt\int_{-\infty}^{\infty} ds\left[\frac{g_{w\omega_0}(|t-s|)}{|\mathbf{r}(t) - \mathbf{r}(s)|^{-2}} + \frac{g^*_{w\omega_0}(|t-s|)}{|\mathbf{r}'(t) - \mathbf{r}'(s)|^{-2}} - 2\frac{g_{w\omega_0}(t-s)}{|\mathbf{r}'(t) - \mathbf{r}(s)|^{-2}}\right], \tag{22}$$

where C and w are Feynman's variational parameters. $\mathcal{Z}(\boldsymbol{\epsilon}, \boldsymbol{\eta})$ is then approximated by two terms,

$$\begin{aligned}\mathcal{Z}(\boldsymbol{\epsilon}, \boldsymbol{\eta}) &= \int \mathcal{D}\mathbf{r}\, \mathcal{D}\mathbf{r}'\, e^{\frac{i}{\hbar}(S[\mathbf{r}]-S[\mathbf{r}']+\Phi[\mathbf{r},\mathbf{r}'])} \\ &\approx \int \mathcal{D}\mathbf{r}\, \mathcal{D}\mathbf{r}'\, e^{\frac{i}{\hbar}(S[\mathbf{r}]-S[\mathbf{r}']+\Phi_0[\mathbf{r},\mathbf{r}'])} \\ &\quad \times \left[1 + \frac{i}{\hbar}\big(\Phi[\mathbf{r},\mathbf{r}'] - \Phi_0[\mathbf{r},\mathbf{r}']\big)\right] \\ &\equiv \mathcal{Z}_0 + \mathcal{Z}_1. \end{aligned} \tag{23}$$

In FHIP and Devreese *et al.* [27] they find that it is more accurate to use the complex impedance function over the complex conductivity $\sigma(\Omega)$ [$= 1/z(\Omega)$] by taking the Taylor expansion of the impedance

$$\begin{aligned}\Omega z(\Omega) = \frac{1}{G(\Omega)} &\approx \frac{1}{G_0(\Omega) + G_1(\Omega)} \\ &\approx \frac{1}{G_0(\Omega)} - \frac{1}{G_0^2(\Omega)} G_1(\Omega), \end{aligned} \tag{24}$$

where G_0 and G_1 are the classical and first-order quantum correction response functions obtained from $\mathcal{Z}_0$ and $\mathcal{Z}_1$, respectively.

This expansion of the impedance gives

$$z(\Omega) \approx i\left(\Omega - \frac{\chi(\Omega)}{\Omega}\right), \tag{25}$$

where

$$\chi(\Omega) = \frac{2\alpha\omega_0^2}{3\sqrt{\pi}} \int_0^\infty dt\ (1 - e^{i\Omega t}) \mathrm{Im} S(t) \tag{26}$$

is a memory function that contains all the first-order corrections from the electron-phonon interactions [Eq. (35a) in FHIP].

Here $S(t)$ [Eq. (35b) in FHIP] is proportional to the dynamic structure factor for the electron and is given by

$$S(t) = g_{\omega_0}(t)[D(t)]^{-\frac{3}{2}}, \tag{27}$$

where

$$\begin{aligned} D(t) = 2\frac{v^2 - w^2}{v^3} &\frac{\sin(v\omega_0 t/2)\sin(v\omega_0[t - i\hbar\beta])}{\sinh(v\omega_0\hbar\beta/2)} \\ &- i\frac{w^2}{v^2}\omega_0 t\left(1 - \frac{t}{i\hbar\beta}\right). \end{aligned} \tag{28}$$

Our $D(t)$ is the same as $D(u)$ in Eq. (35c) in FHIP. The frequency-dependent mobility $\mu(\Omega)$ is obtained from the impedance by using

$$\begin{aligned}\mu(\Omega) &= \mathrm{Re}\left\{\frac{1}{z(\Omega)}\right\} \\ &= \frac{e}{m^*} \frac{\Omega\, \mathrm{Im}\chi(\Omega)}{\Omega^4 - 2\,\Omega^2\, \mathrm{Re}\chi(\Omega) + |\chi(\Omega)|^2}, \end{aligned} \tag{29}$$

where the values of the variational parameters v and w are those that minimize the polaron free energy in Eq. (8). In the limit that the frequency $\Omega \to 0$ gives the FHIP dc mobility,

$$\mu_{\mathrm{dc}}^{-1} = \frac{m^*}{e} \lim_{\Omega\to 0} \frac{\mathrm{Im}\chi(\Omega)}{\Omega} \tag{30}$$

since $\mathrm{Re}\chi(\Omega = 0) = 0$.

C. Numerical evaluation of the memory function

In summary, the integral for the memory function is

$$\chi(\Omega) = \frac{2\alpha\omega_0^2}{3\sqrt{\pi}} \int_0^\infty dt(1 - e^{i\Omega t})\mathrm{Im}S(t), \tag{31a}$$

$$S(t) = \frac{\cos[\omega_0(t - i\hbar\beta/2)]}{\sinh(\hbar\omega_0\beta/2)}[D(t)]^{-\frac{3}{2}}, \tag{31b}$$

$$\begin{aligned} D(t) = 2\frac{v^2 - w^2}{v^3} &\frac{\sin(v\omega_0 t/2)\sin[v\omega_0(t - i\hbar\beta)]}{\sinh(v\omega_0\hbar\beta/2)} \\ &- i\frac{w^2}{v^2}\omega_0 t\left(1 - \frac{t}{i\hbar\beta}\right), \end{aligned} \tag{31c}$$

where Ω is the angular frequency of the driving electric field, ω_0 is the angular phonon frequency, $\beta = 1/k_B T$ is the thermodynamic temperature, and v and w are variational parameters whose values minimize the polaron free energy. This is the same as Eqs. (35) in FHIP, but in SI units and with an alternative algebra.

Previous work [12,27], including our own (see Appendixes), made use of the "doubly oscillatory" contour-rotated integral for the complex memory function in Eq. (26). The imaginary component of the memory function is [Eqs. (47) in Ref. [12]]

$$\begin{aligned}\mathrm{Im}\chi(\Omega) = \frac{2\alpha\omega_0^2}{3\sqrt{\pi}} &\frac{(\hbar\omega_0\beta)^{\frac{3}{2}}\sinh(\hbar\Omega\beta/2)}{\sinh(\hbar\omega_0\beta/2)}\left(\frac{v}{w}\right)^3 \\ &\times \int_0^\infty d\tau \frac{\cos(v\omega_0\tau)\cos(\omega_0\tau)}{\left[\omega_0^2\tau^2 + a^2 - b\,\cos(v\omega_0\tau)\right]^{\frac{3}{2}}}, \end{aligned} \tag{32}$$

where $a^2 \equiv (\hbar\omega_0\beta/2)^2 + R\hbar\beta\omega_0 \coth(\hbar\beta\omega_0 v/2)$, $b \equiv R\hbar\beta\omega_0/\sinh(\hbar\beta\omega_0 v/2)$, and $R \equiv (v^2 - w^2)/(w^2 v)$, and where τ labels *imaginary time* compared to t that labels *real* time in Eqs. (26). Additionally, the contour integral for the real component of the memory function, derived by us (see Appendix A), is

$$\begin{aligned}\mathrm{Re}\chi(\Omega) = \frac{2\alpha\omega_0^2}{3\sqrt{\pi}} &\frac{(\hbar\omega_0\beta)^{\frac{3}{2}}}{\sinh(\hbar\omega_0\beta/2)}\left(\frac{v}{w}\right)^3 \left\{\sinh\left(\frac{\hbar\Omega\beta}{2}\right)\right. \\ &\times \int_0^\infty d\tau \frac{\sin(\Omega\tau)\cos(\omega_0\tau)}{[\omega_0\tau^2 + a^2 - b\,\cos(v\omega_0\tau)]^{\frac{3}{2}}} \\ &\left. - \int_0^{\frac{\hbar\beta}{2}} d\tau \frac{1 - \cosh[\Omega(\tau - \hbar\beta/2)]\cosh(\omega_0\tau)}{\left[a^2 - \omega_0^2\tau^2 - b\,\cosh(v\omega_0\tau)\right]^{\frac{3}{2}}}\right\}. \end{aligned} \tag{33}$$

The imaginary component of the memory function can be expanded in Bessel functions (originally the derivation was outlined in Refs. [10,27], but in Appendix B we provide an in-depth derivation) and the real component in terms of Bessel and Struve functions (see Appendix C for a derivation of the expansion that we believe to be new).

However, we found that the cost of evaluating these expansions became large at low temperatures, requiring arbitrary-precision numerics to slowly reach converged solutions. In Devreese *et al.* [27], they found an alternative analytic expansion for the real component, but similarly found it to have poor convergence for all temperatures, opting instead to transform the integrand to one that has better convergence.

Instead of using any of the contour integrals or power-series expansions, we found that directly numerically integrating Eq. (31) using an adaptive Gauss-Kronrod quadrature algorithm leads to faster convergence and controlled errors. Asymptotic limits of these contour integral expansions, especially at low temperatures, may still prove useful.

III. "BEYOND QUASIPARTICLE" POLARON MOBILITY

Mishchenko *et al.* [26] recently used diagrammatic Monte Carlo (diagMC) calculations to investigate the violation of the so-called "thermal" analog to the Mott-Ioffe-Regel (MIR) criterion in the Fröhlich polaron model. This "thermal" MIR criterion is perhaps better referred to as the *Planckian bound* [31] under which a quasiparticle is stable to inelastic scattering. For the quasiparticle to propagate coherently, the inelastic scattering time τ_{inel} must be greater than the "Planckian time" $\tau_{\text{Pl}} = \hbar/k_B T$. For the polaron mobility μ, this requires $\mu \gtrsim \frac{e\hbar}{Mk_BT}$. This Planckian bound can be reformulated into Mishchenko's [26] "thermal" MIR criterion for the validity of the Boltzmann kinetic equation, $l \gg \lambda$ where l is the mean free path, and λ the de Broglie wavelength, of the charge carrier.

The antiadiabatic limit ($k_BT \ll \hbar\omega_0$) corresponds to the weak-coupling limit ($\alpha \ll 1$), where the perturbative theory result for the mobility is [Eq. (5) in Ref. [26]]

$$\mu = \frac{e}{2M\alpha\omega_0} e^{\hbar\omega_0/k_BT} = \frac{e}{2m^*\omega_0}\left(\frac{1}{\alpha} - \frac{1}{6}\right) e^{\hbar\omega_0/k_BT} \quad (k_BT \ll \hbar\omega_0, \alpha \ll 1), \tag{34}$$

where $M = m^*/(1 - \alpha/6)$ is the effective mass renormalization of the polaron. In the adiabatic regime ($k_BT \gg \hbar\omega_0$), the mobility is obtained from the kinetic equation as [Eq. (6) in Ref. [26]]

$$\mu = \frac{4e\sqrt{\hbar}}{3\sqrt{\pi}\alpha M\sqrt{\omega_0 k_B T}} \quad (k_BT \gg \hbar\omega_0), \tag{35}$$

which is valid even when α is not small.

Figure 1 is a comparison with Fig. 2 in Mishchenko *et al.* [26] of the polaron mobility at $\alpha = 2.5$. At low temperatures ($k_BT \lesssim \hbar\omega_0/2$), the exponential behavior matches the low-temperature mobility in Eq. (34). As in [26], there appears to be a delay in the onset of the exponential behavior for $k_BT < \hbar\omega_0$. Likewise, the MIR criterion is violated over the temperature range $0.2 < k_BT/\hbar\omega_0 < 10$. At high temperatures, the FHIP mobility [Eq. (29)] has the same $1/\sqrt{T}$ dependence as Eq. (35). Figure 2 shows a similar comparison for $\alpha = 4.0$, with unpublished data provided by the authors of [26].

In Fig. 3 we compare the temperature dependence of the FHIP polaron mobility with the diagMC polaron mobility

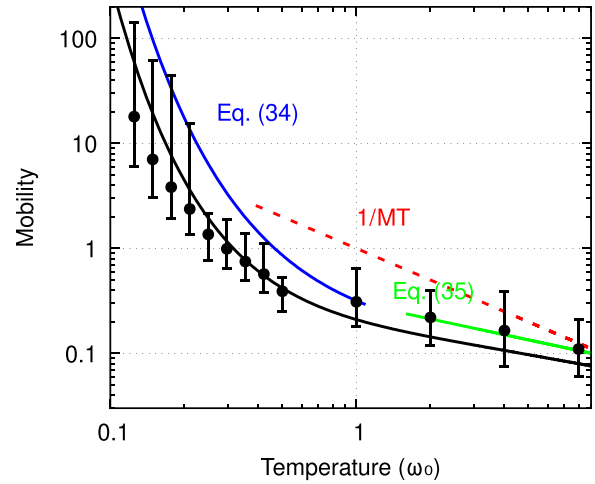

FIG. 1. The FHIP temperature-dependent mobility for the intermediate coupling regime $\alpha = 2.5$ (black, solid), as a comparison to Mishchenko *et al.* [26], Fig. 2 (black dots, with Monte Carlo sampling error bars). This electron-phonon coupling strength is most relevant for moderately polar semiconductors. Following Mishchenko, the blue solid line shows the antiadiabatic and weak-coupling limit of the mobility provided by Eq. (34) [Eq. (5) in [26]]. The green solid line shows the adiabatic limit of the mobility provided by Eq. (35)] Eq. (6) in [26]]. The red dashed line shows the MIR criterion. The FHIP method shows good agreement with the limiting behavior and is within the Monte Carlo sampling error of Mishchenko *et al.* [26]. Already at these relatively weak couplings, the true mobility is well below the MIR independent-scattering criterion. This calls into question the use of the Boltzmann transport equation in simulating even moderately polar materials.

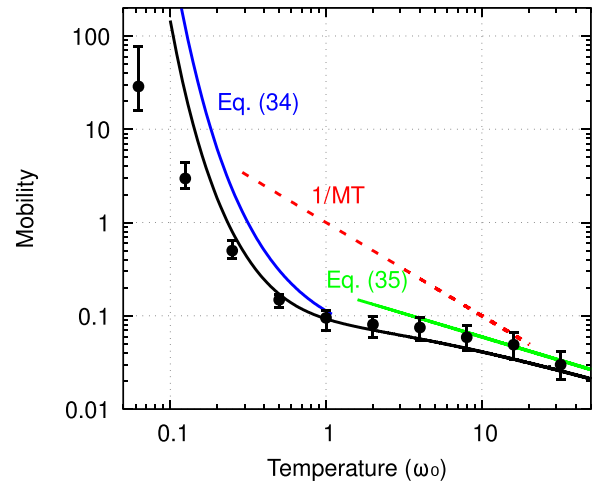

FIG. 2. The FHIP temperature-dependent mobility for the intermediate coupling regime $\alpha = 4.0$ (black, solid), as a comparison to Mishchenko *et al.* [26], Fig. 2 (black dots, with Monte Carlo sampling error bars). This electron-phonon coupling strength is most relevant for strongly polar semiconductors. Following Mishchenko, the blue solid line shows the antiadiabatic and weak-coupling limit of the mobility provided by Eq. (34) [Eq. (5) in [26]]. The green solid line shows the adiabatic limit of the mobility provided by Eq. (35) [Eq. (6) in [26]]. The red dashed line shows the MIR criterion. The FHIP mobility shows good agreement with the limiting adiabatic and antiadiabatic behavior and is clearly away from the MIR criterion where the Boltzmann transport equation is valid.

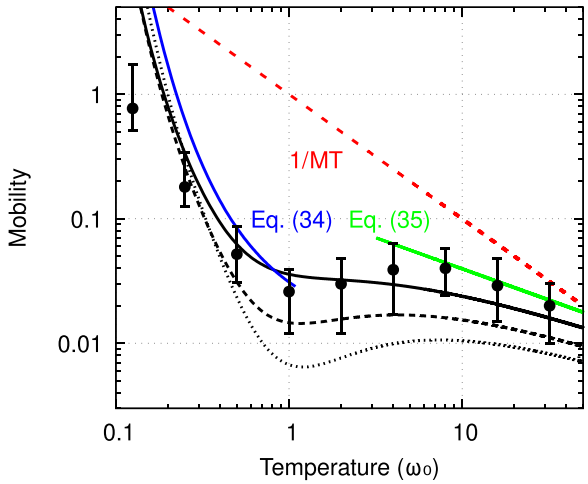

FIG. 3. The FHIP temperature-dependent mobility in the strong-coupling limit is presented as a comparison to Mishchenko *et al.* [26], Fig. 3 (black dots, with Monte Carlo sampling error bars). Presented are $\alpha = 6$ (black, solid), $\alpha = 8$ (black, dashed), $\alpha = 10$ (black, dotted). The diagrammatic Monte Carlo results (black, dots, with Monte Carlo sampling error bars) show pronounced nonmonotonic behavior (the hump at $k_BT/\hbar\omega_0 = 8$) already with $\alpha = 6$, while the FHIP model requires a stronger coupling, though we note that the $\alpha = 6$ FHIP result is within the Monte Carlo error bars.

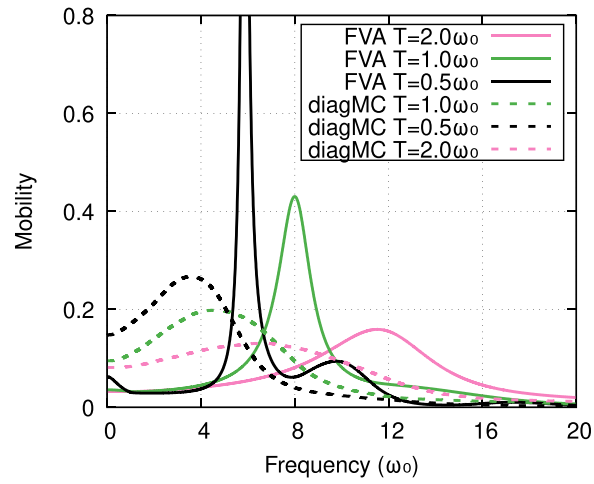

FIG. 4. The FHIP (solid) frequency- and temperature-dependent mobility, presented as a comparison to Mischenko *et al.* [26] (dashed). Presented is $\alpha = 6$ for temperatures $k_BT/\hbar\omega_0 = 0.5$ (black), 1.0 (green), and 2.0 (pink).

(Fig. 3 in Mishchenko *et al.* [26]) at $\alpha = 6$. The diagMC polaron mobility exhibits nonmonotonic behavior at $\alpha = 6$, with a clear local minimum around $k_BT = \hbar\omega_0$. Here we see similar nonmonotonic behavior in the FHIP mobility with a small local minimum appearing around $k_BT = \hbar\omega_0$ too. However, compared to the diagMC mobility, the local minimum of the FHIP mobility is shallower. The onset of this minimum in the FHIP mobility begins around $\alpha = 6$, with the minimum deepening at stronger couplings ($\alpha = 8$ and 10). Similar to the diagMC mobility, the high-temperature limit is recovered after a maximum at $k_BT/\hbar\omega_0 \sim \alpha$ which shifts with larger α. The minimum too appears to be α dependent, occurring at $k_BT/\hbar\omega_0 \sim 1$ for $\alpha = 6$ or $k_BT/\hbar\omega_0 \sim 1.5$ for $\alpha = 10$.

In Fig. 4 we compare the temperature and frequency dependence of the FHIP polaron mobility with the diagMC polaron mobility (Fig. 4 in Mishchenko *et al.* [26]) at $\alpha = 6$ for temperatures $T = 0.5\omega_0, 1.0\omega_0, 2.0\omega_0$. The FHIP mobility, obtained by integrating Eq. (29), has similar temperature dependence to the diagMC mobility but differs in frequency response.

The FHIP mobility shows extra peaks where the first peak is blueshifted compared to the diagMCs single peak. In [27,32] it is shown that these extra peaks of the FHIP mobility correspond to internal relaxed excited states of the polaron quasiparticle. These internal states correspond to multiple phonon scattering processes. For $k_BT/\hbar\omega_0 = 0.5$, the first peak around $\Omega/\omega_0 \sim 6$ corresponds to one-phonon processes, the peak at $\Omega/\omega_0 \sim 10$ corresponds to two-phonon processes, and so on. This is more clearly seen by analyzing the memory function $\chi(\Omega)$ [Eq. (26)] at zero temperature, which similarly has peaks at $\Omega/\omega_0 = 1 + nv$, where $n = 0, 1, 2, \ldots$, and v is one of the Feynman variational parameters (cf. Fig. 5). These peaks in the memory function correspond to the same Frank-Condon states. As the temperature increases, the first few peaks become more prominent and broaden due to an increased effective electron-phonon interaction. Eventually, the excitations can no longer be resolved at high temperatures.

The Feynman variational model of the electron harmonically coupled to a fictitious massive particle (cf. Sec. VI) lacks a dissipative mechanism for the polaron such that the polaron state described by this model does not lose energy and has an infinite lifetime. However, in de Filippis *et al.* [32], dissipation is included in this model at zero temperature. This attenuates and spreads the harmonic peaks, obscuring the internal polaron transitions, giving closer agreement to the diagMC mobility at zero temperature. We have not used these

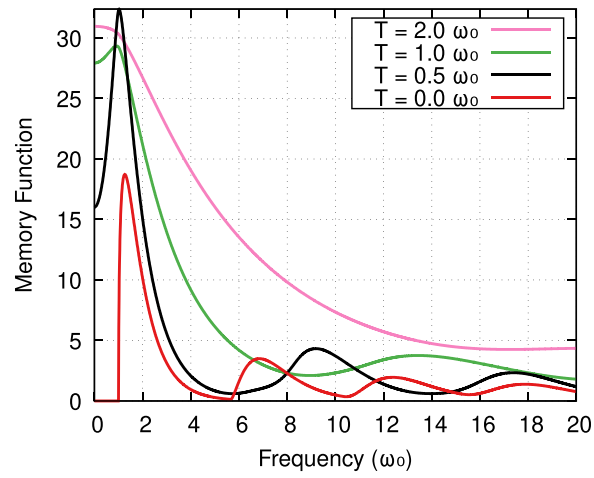

FIG. 5. The frequency and temperature dependence of the memory function χ [Eq. (26)]. The peaks correspond to the Frank-Condon states of the polaron. For zero temperature $k_BT/\hbar\omega_0 = 0.0$ (red) the variational parameter $v = 4.67$ such that the peaks occur after $\omega_0 + nv\omega_0 = \omega_0, 5.67\omega_0, 10.33\omega_0$, etc. At higher temperatures, the peaks shift to higher frequencies due to the temperature dependence of v that minimizes the polaron free energy at a given temperature.

methods here but they will be investigated in future work to complement the multiple phonon model action with a more generalized trial action.

IV. EXTENDING THE FRÖHLICH MODEL

A. Multiple phonon mode electron-phonon coupling

In simple cubic polar materials with two atoms in the unit cell, the single triply degenerate optical phonon branch is split by dielectric coupling into the singly degenerate longitudinal-optical (LO) mode and double-generate transverse-optical (TO) modes. Only the longitudinal-optical mode is infrared active and contributes to the Fröhlich dielectric electron-phonon interaction.

The infrared activity of this mode drives the formation of the polaron. Much of the original literature therefore just refers to *the* LO mode. In a more complex material, the full range of infrared active modes all contribute to the polaron stabilization, and the infrared activity of these modes is no longer severely restricted by group theory, but are instead best evaluated numerically. The driving force of the infrared activity is, however, slightly obscured by the algebra in Eq. (3), and instead, this electron-phonon coupling seems to emerge from the bulk properties of the lattice. The Pekar factor $\frac{1}{\epsilon_{\text{optic}}} - \frac{1}{\epsilon_{\text{static}}}$ is particularly opaque.

Rearranging the Pekar factor as

$$\left(\frac{1}{\epsilon_{\text{optic}}} - \frac{1}{\epsilon_{\text{static}}}\right) = \frac{\epsilon_{\text{ionic}}}{\epsilon_{\text{optic}}\epsilon_{\text{static}}}, \tag{36}$$

we can now see that the Fröhlich α is proportional to the ionic dielectric contribution, as would be expected from appreciating that this is the driving force for polaron formation.

The static dielectric constant is the sum of the high-frequency ("optical") response of the electronic structure and the lower-frequency vibrational response of the ions $\epsilon_{\text{static}} = \epsilon_{\text{optic}} + \epsilon_{\text{ionic}}$. This vibrational contribution is typically calculated [33] by summing the infrared activity of the individual harmonic modes as Lorentz oscillators. This infrared activity can be obtained by projecting the Born effective charges along the dynamic matrix (harmonic phonon) eigenvectors. The overall dielectric function across the phonon frequency range can be written as

$$\begin{aligned}\epsilon(\Omega) &= \epsilon_{\text{optic}} + \sum_{j=1}^{m} \epsilon_j(\Omega) \\ &= \epsilon_{\text{optic}} + \frac{4\pi}{\Omega_0} \sum_{j=1}^{m} \frac{(U\cdot q)\cdot(U\cdot q)}{\omega_j^2 - \Omega^2}.\end{aligned} \tag{37}$$

Here U are the dynamic matrix eigenvectors, Ω is the reduced frequency of interest, ω_j is the phonon reduced frequency, Ω_0 is the unit-cell volume, q are the Born effective charges, j indexes the jth phonon branch, and m is the total number of phonon branches.

Considering the isotropic case (and therefore picking up a factor of $\frac{1}{3}$ for the averaged interaction with a dipole), and expressing the static (zero-frequency) dielectric contribution, in terms of the infrared activity of a mode ϵ_j is

$$\epsilon_j(0) = \frac{4\pi}{\Omega_0}\frac{1}{3}\frac{\kappa_j^2}{\omega_j^2}\, q^2/u, \tag{38}$$

where κ is the infrared activity in the standard unit of the electron charge (q) squared per atomic mass unit (u).

This provides a clear route to defining α_j for individual phonon branches, with the simple constitutive relationship that $\alpha = \sum_j \alpha_j$:

$$\alpha_j = \frac{1}{4\pi\epsilon_0}\frac{\epsilon_j}{\epsilon_{\text{optic}}\epsilon_{\text{static}}}\frac{e^2}{\hbar}\left(\frac{m^*}{2\hbar\omega_j}\right)^{\frac{1}{2}}. \tag{39}$$

This concept of decomposing α into constituent pieces associated with individual phonon modes is implicit in the effective mode scheme of Hellwarth and Biaggio [21], and has also been used by Verdi [34], Verbist [35], and Devreese *et al.* [36].

B. Multiple phonon mode path integral

Verbist and Devreese [35] proposed an extended Fröhlich model Hamiltonian [Eq. (1)] with a sum over multiple (m) phonon branches:

$$\begin{aligned}\hat{H} = \frac{p^2}{2m^*} &+ \sum_{\mathbf{k},j} \hbar\,\omega_j\, a^\dagger_{\mathbf{k},j} a_{\mathbf{k},j} \\ &+ \sum_{\mathbf{k},j} (V_{\mathbf{k},j}\, a_{\mathbf{k},j}\, e^{i\mathbf{k}\cdot\mathbf{r}} + V^*_{\mathbf{k},j}\, a^\dagger_{\mathbf{k},j}\, e^{-i\mathbf{k}\cdot\mathbf{r}}).\end{aligned} \tag{40}$$

Here the index j indicates the jth phonon branch. The interaction coefficient is given by

$$V_{\mathbf{k},j} = i\frac{2\hbar\omega_j}{|\mathbf{k}|}\left(\sqrt{\frac{\hbar}{2m^*\omega_j}}\frac{\alpha_j\pi}{\Omega_0}\right)^{\frac{1}{2}}, \tag{41}$$

with α_j as in Eq. (39).

From this Hamiltonian, we provide the following extended model action to use within the Feynman variational theory:

$$\begin{aligned}S_j[\mathbf{r}(\tau)] = \frac{m^*}{2}\int_0^{\hbar\beta} d\tau \left(\frac{d\mathbf{r}(\tau)}{d\tau}\right)^2 \\ - \frac{(\hbar\omega_j)^{\frac{3}{2}}}{2\sqrt{2m^*}}\alpha_j \int_0^{\hbar\beta} d\tau \int_0^{\hbar\beta} d\sigma\, \frac{g_{\omega_j}(|\tau-\sigma|)}{|\mathbf{r}(\tau)-\mathbf{r}(\sigma)|}.\end{aligned} \tag{42}$$

Here $g_{\omega_j}(\tau)$ is the imaginary-time phonon Green's function for a phonon with frequency ω_j:

$$g_{\omega_j}(\tau) = \frac{\cosh\left[\omega_j(\tau - \hbar\beta/2)\right]}{\sinh\left(\hbar\omega_j\beta/2\right)}. \tag{43}$$

This form of action is consistent with Hellwarth and Biaggio's [21] deduction that inclusion of multiple phonon branches gives the interaction term simply as a sum over terms with phonon frequency ω_j and coupling constant α_j dependencies.

We now choose a suitable trial action to use with the action in Eq. (42). We use Feynman's original trial action with two variational parameters, C and w, which physically represent a particle (the charge carrier) coupled harmonically to a single

fictitious particle (the additional mass of the quasiparticle due to interaction with the phonon field) with a strength C and a frequency w.

Clearly, the dynamics of this model cannot be more complex than can be arrived at with the original Feynman theory, though the direct variational optimization (at each temperature) may get closer than using Hellwarth and Biaggio's [21] effective phonon mode approximation.

C. Multiple phonon mode free energy

We extend Hellwarth and Biaggio's A, B, and C equations [Eqs. (62b), (62c), and (62e) in Ref. [21]) (presented here with explicit units)

$$A = \frac{3}{\hbar\beta\omega_0}\left[\log\left(\frac{w\,\sinh(v\hbar\beta\omega_0/2)}{v\,\sinh(w\hbar\beta\omega_0/2)}\right) - \frac{1}{2}\log(2\pi\hbar\beta\omega_0)\right], \tag{44a}$$

$$B = \frac{\alpha\omega_0}{\sqrt{\pi}}\int_0^{\frac{\hbar\beta}{2}} d\tau\, g_{\omega_0}(\tau)[D(\tau)]^{-\frac{1}{2}}, \tag{44b}$$

$$C = \frac{3}{4}\frac{v^2-w^2}{v}\left[\coth\left(\frac{v\hbar\beta\omega_0}{2}\right) - \frac{2}{v\hbar\beta\omega_0}\right] \tag{44c}$$

to multiple phonon modes, where $D(\tau)$ is given in Eq. (28). Hellwarth and Biaggio's B is a symmetrized (for ease of computation) version of the equivalent term from Ōsaka [17], although here we have unsymmetrized the integral in B to condense the notation. Compared to Ōsaka, B and C are related to the expectation value of the model action $\langle S\rangle_0$ and trial action $\langle S_0\rangle_0$, respectively, and A is the free energy derived from the trial partition function $F_0 = -\log(Z_0)/\beta$. Following the procedure of Ōsaka [17], from the multiple phonon action in Eq. (42) we derive the phonon-mode-dependent A_j and C_j equations

$$A_j = \frac{3}{\hbar\omega_j\beta}\left[\log\left(\frac{v\,\sinh(w\hbar\omega_j\beta/2)}{w\,\sinh(v\hbar\omega_j\beta/2)}\right) - \frac{1}{2}\log\left(2\pi\hbar\omega_j\beta\right)\right], \tag{45a}$$

$$C_j = \frac{3}{4}\frac{v^2-w^2}{v}\left[\coth\left(\frac{v\hbar\omega_j\beta}{2}\right) - \frac{2}{v\hbar\omega_j\beta}\right]. \tag{45b}$$

Similarly, we derive a multiple phonon mode extension to Hellwarth and Biaggio's B expression

$$B_j = \frac{\alpha_j\omega_j}{\sqrt{\pi}}\int_0^{\frac{\hbar\beta}{2}} d\tau\, g_{\omega_j}(\tau)[D_j(\tau)]^{-\frac{1}{2}}, \tag{46}$$

where

$$D_j(\tau) = 2\frac{v^2-w^2}{v^3}\frac{\sinh\left(v\omega_j\tau/2\right)\sinh\left(v\omega_j[\hbar\beta-\tau]/2\right)}{\sinh(v\hbar\omega_j\beta/2)} + \left(1-\frac{v^2-w^2}{v^2}\right)\tau\omega_j\left(1-\frac{\tau}{\hbar\beta}\right). \tag{47}$$

These are similar to Hellwarth and Biaggio's single-mode versions, but with the single effective phonon frequency ω_0 substituted with the branch-dependent phonon frequencies ω_j. There are m with index j phonon branches.

Summing A_j in Eq. (45a), B_j in Eq. (46), and C_j in Eq. (45b), we obtain a generalized variational inequality for the contribution to the free energy of the polaron from the jth phonon branch with phonon frequency ω_j and coupling constant α_j, and two variational parameters v and w:

$$F(\beta) \leqslant -\sum_{j=1}^{m}\hbar\omega_j(A_j + C_j + B_j). \tag{48}$$

Here we have taken care to write out the expression explicitly, rather than use "polaron" units. The entire sum on the right-hand side of Eq. (48) must be minimized simultaneously to ensure we obtain a single pair of v and w parameters that give the lowest upper bound for the total model free energy F.

We obtain variational parameters v and w that minimize the free-energy expression and will be used in evaluating the polaron mobility. When we consider only one phonon branch ($m = 1$) this simplifies to Hellwarth and Biaggio's form of Ōsaka's free energy. Feynman's original athermal version can then be obtained by taking the zero-temperature limit ($\beta \to \infty$).

D. Multiple phonon mode complex mobility

To generalize the frequency-dependent mobility in Eq. (29), we follow the same procedure as FHIP, but use our generalized polaron action S [Eq. (42)] and trial action S_0 [Eq. (7)]. The result is a memory function akin to FHIP's χ [Eq. (26)] that now includes multiple (m) phonon branches j:

$$\chi_{\text{multi}}(\Omega) = \sum_{j=1}^{m}\frac{\alpha_j\omega_j^2}{3\sqrt{\pi}}\int_0^{\infty} dt\,[1-e^{i\Omega t}]\text{Im}S_j(t). \tag{49}$$

Here,

$$S_j(\Omega) = g_{\omega_j}(t)[D_j(t)]^{-\frac{3}{2}}, \tag{50}$$

where $D_j(t)$ is $D_j(\tau = -it)$ from Eq. (47) rotated back to real time to give a generalized version of $D(u)$ in Eq. (35c) in FHIP:

$$D_j(t) = 2\frac{v^2-w^2}{v^3}\frac{\sin(v\omega_j t/2)\sin(v\omega_j[t-i\hbar\beta]/2)}{\sinh(v\omega_j\hbar\beta/2)} - i\left(1-\frac{v^2-w^2}{v^2}\right)t\omega_j\left(1-\frac{t}{i\hbar\beta}\right). \tag{51}$$

The new multiple phonon frequency-dependent mobility $\mu_{\text{multi}}(\Omega)$ is then obtained from the real and imaginary parts of the generalized $\chi_{\text{multi}}(\Omega)$ using Eq. (29).

V. COMPARISON BETWEEN EFFECTIVE MODE AND MULTIPLE MODE THEORIES

Having extended the Feynman theory with explicit phonon modes in the *model* action, we must now try and answer what improvement this makes.

Halide perovskites are relatively new semiconductors of considerable technical interest. They host strongly interacting large polarons due to their unusual mix of a light effective mass yet strong dielectric electron-phonon coupling. Recently, the coherent charge-carrier dynamics upon

TABLE I. Parameters of the Feynman polaron model (single effective phonon mode) as used in this work. Relative high-frequency ($\epsilon_{\text{optical}}$) and static ($\epsilon_{\text{static}}$) dielectric constants are given in units of the permittivity of free space (ϵ_0). Frequency (f) is in THz. Effective mass (m^*) is in units of the bare electron mass. These data are as in Ref. [22].

Material	$\epsilon_{\text{optical}}$	ϵ_{static}	f	m^*
$MAPbI_3$-e	4.5	24.1	2.25	0.12
$MAPbI_3$-h	4.5	24.1	2.25	0.15

photoexcitation is being measured, the terahertz spectroscopy showing rich transient vibrational features [38].

Therefore, we choose to use this system as representative of the more complex systems which could be modelled with our extended theory. In what follows, we take the materials data from our 2017 paper [22], which we reproduce here in Table I.

A. Free energy

We compare the polaron free energy and variational parameters evaluated by our explicit phonon frequency method presented in Eq. (48) to Hellwarth and Biaggio's effective phonon frequency scheme [scheme B in Eqs. (58) and (59) in Ref. [21]]

$$\frac{\kappa_{\text{eff}}^2}{\omega_{\text{eff}}^2} = \sum_{j=1}^{m} \frac{\kappa_j^2}{\omega_k^2}, \tag{52a}$$

$$\kappa_{\text{eff}}^2 = \sum_{j=1}^{m} \kappa_j^2, \tag{52b}$$

that use an effective LO phonon mode frequency ω_{eff} and associated infrared oscillator strength κ_{eff} derived from sums over the phonon modes j. We apply both of these methods to the 15 solid-state optical phonon branches of $MAPbI_3$, of which the frequencies and infrared activities are shown in Table II.

TABLE II. Infrared activity (IR) of phonon modes in $MAPbI_3$ taken from Ref. [37], scaled to their ground-state polaron value by the multimodal $w = 2.6792$ factor for $MAPbI_3$-e of this work (Table III).

Base frequency	Polaron frequency	IR activity	α_j
4.02	10.8	0.0817	0.0340
3.89	10.4	0.00631	0.00300
3.53	9.46	0.0535	0.0310
2.76	7.38	0.0213	0.0230
2.44	6.53	0.232	0.336
2.25	6.03	0.262	0.465
2.08	5.57	0.234	0.505
2.03	5.45	0.0623	0.142
1.57	4.20	0.0367	0.161
1.02	2.73	0.0126	0.162
1.00	2.69	0.00682	0.0910
0.997	2.67	0.0104	0.141
0.920	2.47	0.0110	0.182
0.801	2.144	0.00168	0.0400
0.574	1.54	0.00646	0.349

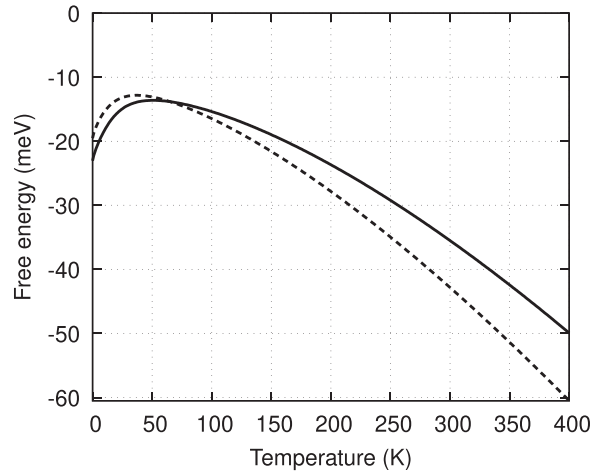

FIG. 6. Comparison of the polaron free energy as a function of temperature for $MAPbI_3$ with the single effective phonon mode approach (solid) and the explicit multiple phonon mode approach (dashed).

Using the Hellwarth and Biaggio [21] effective phonon frequency "B" scheme, the effective phonon frequency for $MAPbI_3$ is $\omega_0 = 2.25 \times 2\pi$ THz and the Fröhlich alpha for $MAPbI_3$-e is $\alpha = 2.39$ and $MAPbI_3$-h is $\alpha = 2.68$, as in our previous work [22] (values from bulk dielectric constants).

Using Eq. (39), we calculated the partial Fröhlich alpha α_j parameters for each of the 15 phonon branches in $MAPbI_3$, which are given in Table II. For $MAPbI_3$-e the partial Fröhlich alphas sum to $\alpha = 2.66$ and for $MAPbI_3$-h they sum to $\alpha = 2.98$. These 15 partial alphas α_j and corresponding phonon frequencies ω_j were then used in the variational principle for the multiple phonon-dependent free energy in Eq. (48). From Eq. (48), we variationally evaluate a v and w parameter.

Figure 6 shows the polaron free-energy comparison. The explicit multiple phonon mode approach predicts a higher free energy at temperatures $T < 65$ K and a lower free energy at temperatures $T > 65$ K. See Table III for our athermal results, where we find new multiple-mode estimates for the polaron binding energy E_b (at 0 K) for $MAPbI_3$-e as $E_b = -19.52$ meV and $MAPbI_3$-h as $E_b = -21.92$ meV. Also see Table IV for our thermal results at $T = 300$ K, where we find new multiple-mode estimates for the polaron free energy F for $MAPbI_3$-e at 300 K as $F = -42.84$ meV and $MAPbI_3$-h as

TABLE III. Athermal 0-K results. Dielectric electron-phonon coupling (α), Feynman athermal variational parameters (v and w), and polaron binding energy (E_b) for an effective phonon mode (top rows) and for multiple explicit phonon modes (bottom rows).

Material	α	v	w	E_b
$MAPbI_3$-e	2.39	3.3086	2.6634	−23.0 meV
$MAPbI_3$-h	2.68	3.3586	2.6165	−25.9 meV
$MAPbI_3$-e	2.66	3.2923	2.6792	−19.5 meV
$MAPbI_3$-h	2.98	3.3388	2.6349	−21.9 meV

TABLE IV. 300-K Results. Dielectric electron-phonon coupling (α), Feynman thermal variational parameters (v and w), polaron free energy (F, meV), dc mobility (μ, cm^2 V^{-1} s^{-1}), polaron effective mass (M, m^*), and Schultz polaron radius (r_f, Å) for an effective phonon mode (top rows) and for multiple explicit phonon modes from Table II (bottom rows).

Material	α	v	w	F	μ	M	r_f
$MAPbI_3$-e	2.39	19.9	17.0	−35.5	136	0.37	43.6
$MAPbI_3$-h	2.68	20.1	16.8	−43.6	94	0.43	36.9
$MAPbI_3$-e	2.66	35.2	32.5	−42.8	160	0.18	44.1
$MAPbI_3$-h	2.98	35.3	32.2	−50.4	112	0.20	37.2

$F = -50.40$ meV. These are to be compared to our previous results in Ref. [22], which are also provided in Tables III and IV.

Figure 7 shows the comparison in polaron variational parameters v and w. That we have different trends for the polaron free energy and variational v and w parameters shows that we find quite a different quasiparticle solution from our multiple phonon scheme compared to the single effective frequency scheme.

B. DC mobility

We calculate the zero-frequency (direct current, dc) electron-polaron mobility μ in $MAPbI_3$ using the effective phonon mode and explicit multiple phonon mode approaches. Both approaches have the same relationship between the mobility and the memory function [Eqs. (29) and (30)], but the effective mode approach uses the memory function $\chi(\Omega)$ from Eq. (26) [the FHIP [12] memory function, Eq. (35) ibid.], whereas the multiple phonon mode approach uses our $\chi_{\text{multi}}(\Omega)$ from Eq. (49) (with a sum over the phonon modes). Figure 8 shows temperatures $0\,K$ to $400\,K$. In Fig. 9 we see that the multiple mode approach corrects the single effective mode approach by up to 20%, with this correction maximized at $T = 140$ K. The multiple-mode mobility slowly approaches the single-mode mobility towards higher temperatures. We assume the divergence towards zero temperature to be a numerical error due to the ratio of large floating-point numbers as both mobility values diverge to positive infinity.

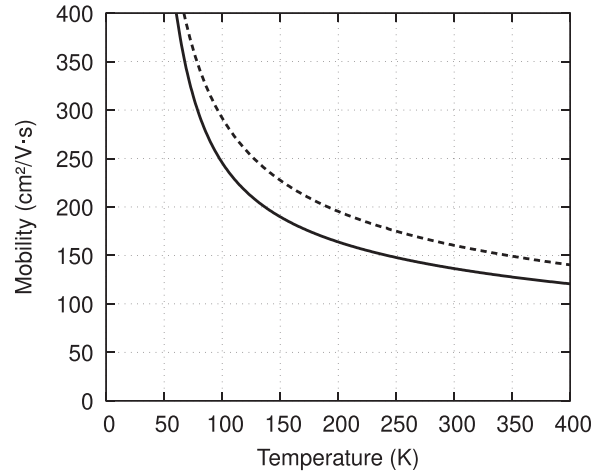

FIG. 8. Comparison of the temperature-dependent mobility predicted for $MAPbI_3$ by the single effective phonon mode approach (solid) and the explicit multiple phonon mode approach (dashed).

C. Complex conductivity and impedance

We calculate the complex impedance $z_{\text{multi}}(\Omega)$ for the polaron in $MAPbI_3$ using Eq. (25), where the only difference between the effective mode and multiple mode approaches is in the form of the memory function $\chi_{\text{multi}}(\Omega)$ as described for the polaron mobility above. The complex conductivity $\sigma_{\text{multi}}(\Omega)$ is the reciprocal of the complex impedance, $\sigma_{\text{multi}}(\Omega) = 1/z_{\text{multi}}(\Omega)$.

We show in Fig. 10 the real component and in Fig. 11 the imaginary component of the complex conductivity for the single effective mode approach (top) and the explicit mul-

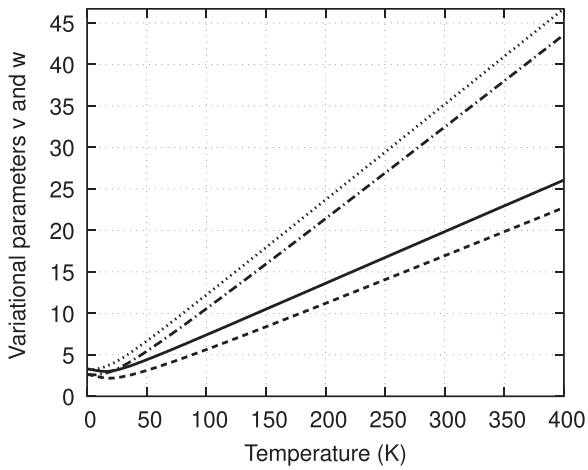

FIG. 7. Comparison of the two polaron variational parameters (v and w) for $MAPbI_3$ in the single effective phonon mode approach (v, solid; w dashed) and the explicit multiple phonon mode approach (v, dots; w dot-dashes).

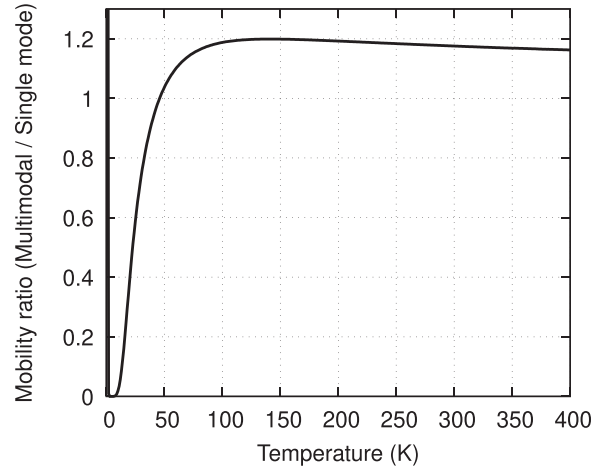

FIG. 9. Ratio of the temperature-dependent mobility predicted for $MAPbI_3$ by the explicit multiple and single effective phonon mode approaches (solid). The multiple mode approach gives up to 20% correction, maximized at $T = 140$ K.

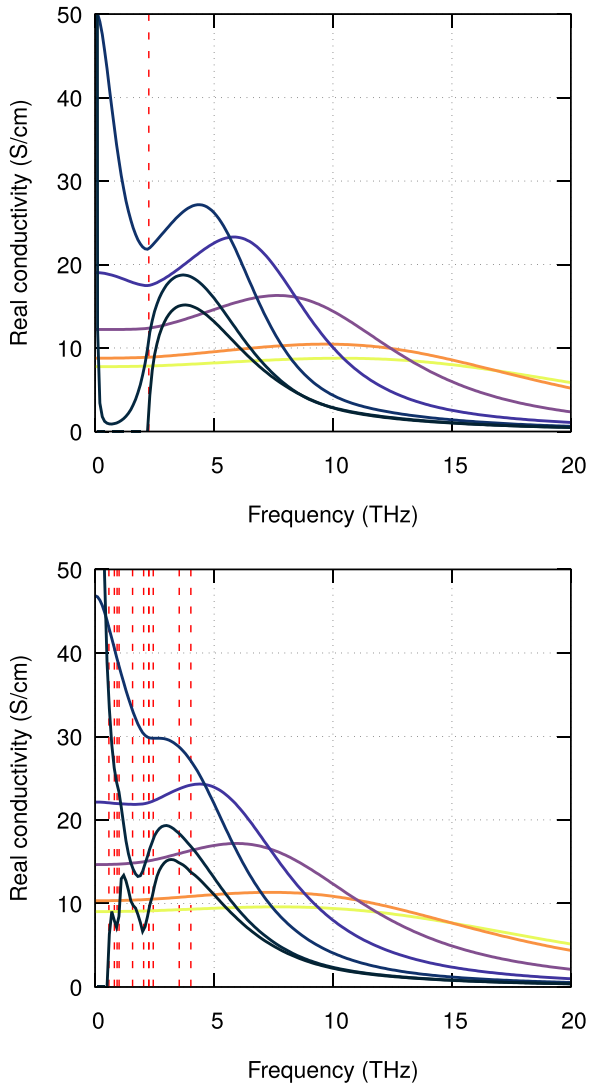

FIG. 10. Real component of the complex conductivity for $MAPbI_3$ for temperatures $T = 0$, 10, 40, 80, 150, 300, and 400 K starting with the black curve and finishing with the yellow curve. (Top) Single effective phonon mode prediction. (Bottom) Explicit multiple phonon mode prediction. The red vertical dashed lines indicate the frequencies of the phonon modes.

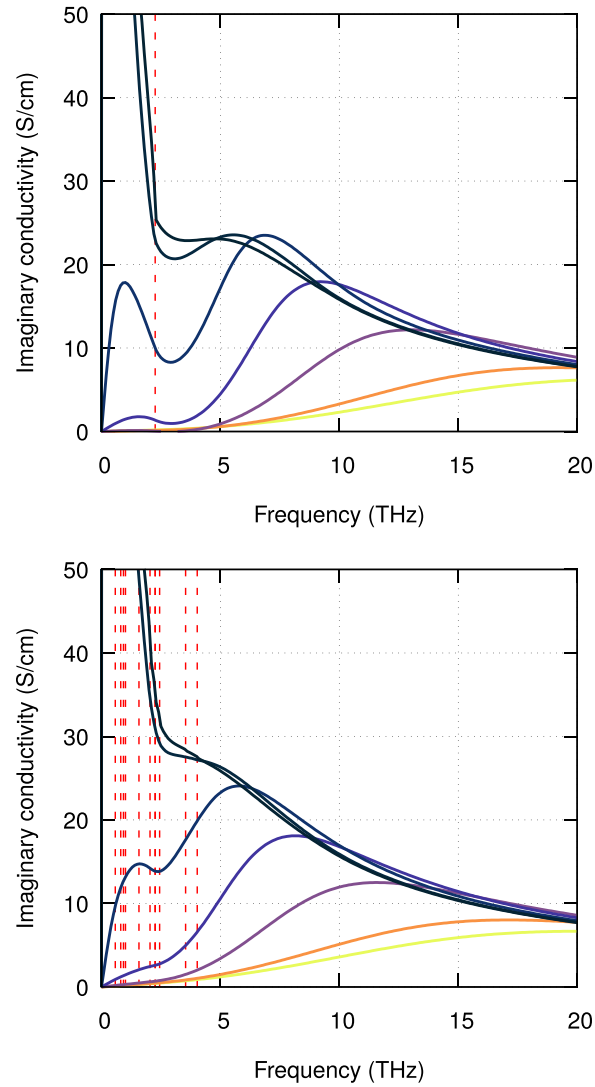

FIG. 11. Imaginary component of the complex conductivity for $MAPbI_3$ for temperatures $T = 0$, 10, 40, 80, 150, 300, and 400 K starting with the black curve and finishing with the yellow curve. (Top) Single effective phonon mode prediction. (Bottom) Explicit multiple phonon mode prediction. The red vertical dashed lines indicate the frequencies of the phonon modes.

tiple mode approach (bottom) for temperatures $T = 0$, 10, 40, 80, 150, 300, and 400 K (starting with the solid black line through to the yellow solid line) and for frequencies $0 \leqslant \Omega \leqslant 20$ THz. The vertical dashed red lines show the LO phonon modes of $MAPbI_3$. The difference between the two approaches is largest at low temperatures $T = 0$ and 10 K where the multiple phonon approach has more structure due to the extra phonon modes. At higher temperatures, the structure attenuates and the two approaches show similar frequency dependence of the complex conductivity at $T = 300$ and 400 K. These features are further reflected in the real and imaginary components of the complex impedance as shown in Figs. 12 and 13, respectively.

In Fig. 14 we specifically show the real and imaginary components of the complex conductivity at zero temperature $T = 0$ K over frequencies $0 \leqslant \Omega \leqslant 5.0$ THz for both approaches. Again, the vertical dashed red lines show the longitudinal-optical (LO) phonon modes of $MAPbI_3$ used in the calculation and are shown in Table II. The single effective mode conductivity shows a peak in the real component at frequencies above the effective mode frequency $\Omega \geqslant 2.25$ THz. Whereas, the real component of the multiple mode conductivity shows peaks at frequencies at and above the LO phonon mode frequencies in $MAPbI_3$. The imaginary components of both approaches show some structure changes at their respective LO phonon mode frequencies but are harder to discern at zero temperature. The most prominent modes in $MAPbI_3$ appear at the large electron-phonon coupled modes $\omega_0 = 0.58$, 1.00, and 2.44 THz.

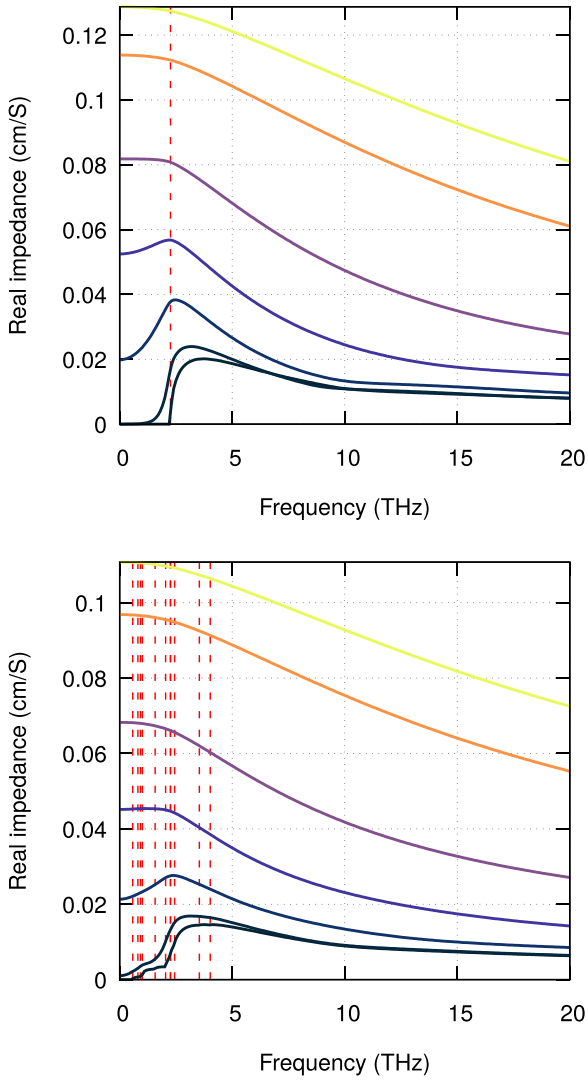

FIG. 12. Real component of the complex impedance for $MAPbI_3$ for temperatures $T = 0$, 10, 40, 80, 150, 300, and 400 K starting with the black curve and finishing with the yellow curve. (Top) Single effective phonon mode prediction. (Bottom) Explicit multiple phonon mode prediction. The red vertical dashed lines indicate the frequencies of the phonon modes.

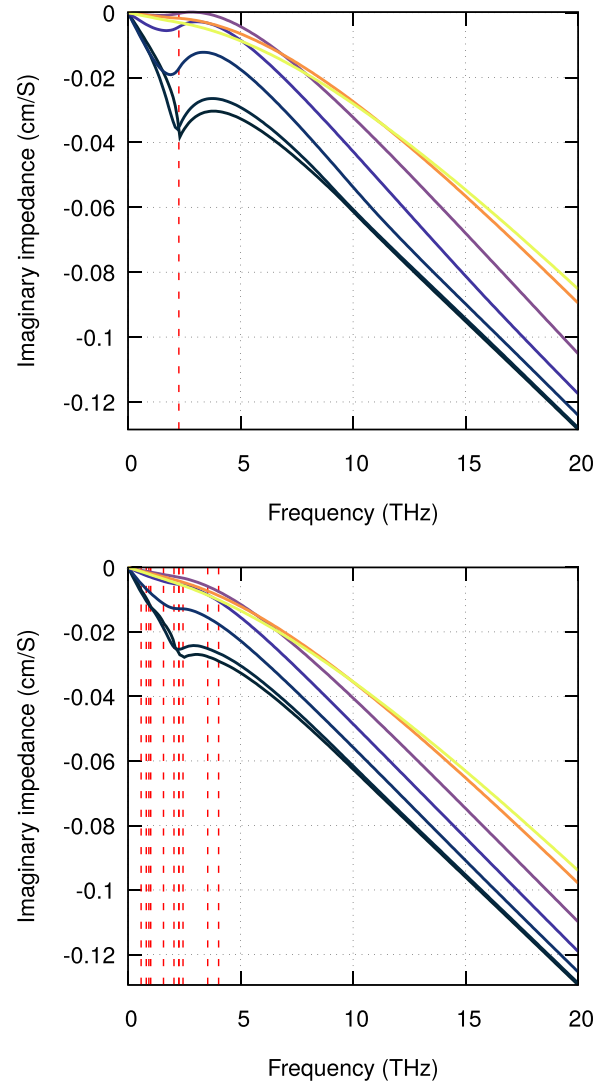

FIG. 13. Imaginary component of the complex impedance for $MAPbI_3$ for temperatures $T = 0$, 10, 40, 80, 150, 300, and 400 K starting with the black curve and finishing with the yellow curve. (Top) Single effective phonon mode prediction. (Bottom) Explicit multiple phonon mode prediction. The red vertical dashed lines indicate the frequencies of the phonon modes.

VI. SIMULATED POLARON VIBRATIONAL MODE SPECTRA

The Feynman polaron quasiparticle has a direct mechanistic interpretation. The Lagrangian consists of an effective-mass electron, an additional fictitious particle (mass M, in units of the electron effective mass), coupled by a harmonic restoring force (k). This Lagrangian is given by

$$L = \frac{m^*}{2}\dot{\mathbf{r}}(t)^2 + \frac{M}{2}\dot{\mathbf{R}}(t)^2 - \frac{k}{2}[\mathbf{r}(t) - \mathbf{R}(t)]^2. \quad (53)$$

The rate of oscillation of this mode is simply $w = \sqrt{\frac{k}{M}}$, expressed as a prefactor to the material phonon frequency. This oscillation describes the coherent exchange of energy between the electron and the phonon field. The phonon frequencies are blueshifted by the electron-phonon coupling. In terms of the variational parameters v and w, the spring constant is $k = v^2 - w^2$ and the fictitious mass is $M = (v^2 - w^2)/w^2$.

Following Schultz [40], the size of the polaron is estimated by calculating the root-mean-square distance between the electron and the fictitious particle, given as $r_f = (\langle \mathbf{r} - \mathbf{R} \rangle)^{\frac{1}{2}} = \sqrt{3v/(v^2 - w^2)}\ a_p$, where the polaron radius is in units of characteristic polaron length $a_p = \sqrt{\hbar/(2m^*\omega_0)}$.

Figure 15 shows the comparison in the polaron effective mass M (units of effective electron mass m^*) and polaron radius r_f (units of characteristic polaron length a_p) applied to $MAPbI_3$. At 300 K we find new estimates of $M = 0.18\ m^*$ and $r_f = 0.755$, $a_p = 44.08$ Å to be compared to $M = 0.37\ m^*$ and $r_f = 0.747$, $a_p = 43.62$ Å (Table IV). While the introduction of multiple phonon modes barely alters the polaron size, we note that it practically halves the polaron's effective mass.

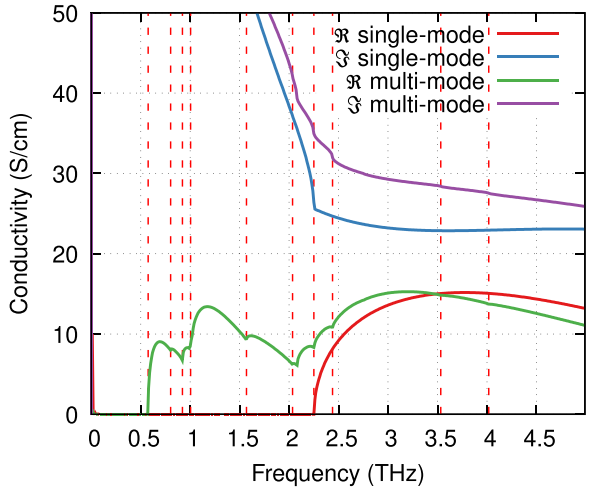

FIG. 14. Comparison between the real and imaginary components of the complex conductivity predicted for $MAPbI_3$ by the single effective phonon mode approach and the explicit multiple phonon mode approach.

The original work of Feynman [10] provides several asymptotic estimates of this w parameter. The standard approximations often reproduced in textbooks are $w = 3$ for small α coupling, and $w = 1$ for large α coupling. Precise work requires a numeric solution, but these limits inform us that the internal polaron mode, as a function of electron-phonon coupling, starts as a harmonic of $3\omega_0$ and continuously redshifts to the phonon fundamental frequency ω_0. These parameters as a function of α are shown in Fig. 16.

The finite-temperature Ōsaka [17] action is also described by the Lagrangian which describes the free energy of the polaron state and has the simple mechanistic interpretation of the electron at position $\mathbf{r}(t)$ coupled by a spring with force constant k to a fictitious particle of mass M at position $\mathbf{R}(t)$. Practically, the finite-temperature action gives rise to a set of v

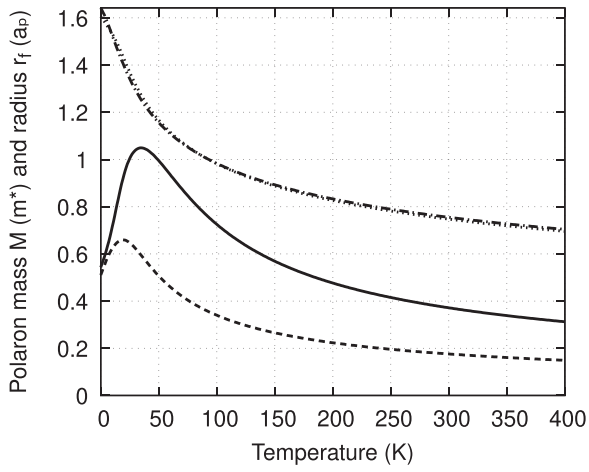

FIG. 15. Comparison of polaron effective mass M (in units of effective band mass m^*) and Schultz polaron radius r_f (in units of characteristic polaron length a_p) for $MAPbI_3$ in the single effective phonon mode approach (M, solid; r_f, dashed) and the explicit multiple phonon mode approach (M, dots; r_f, dotted-dashed).

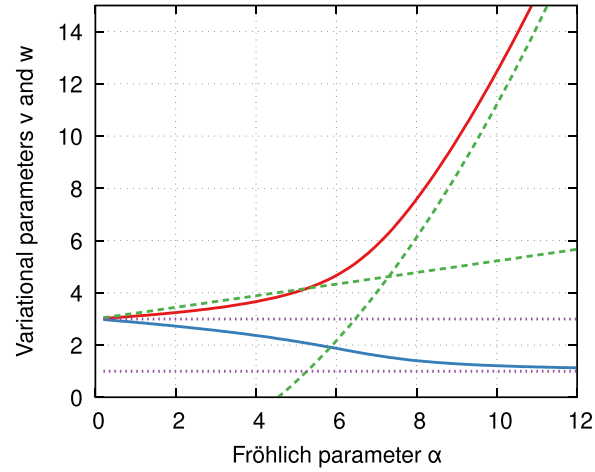

FIG. 16. Numeric Feynman variational solution with the original athermal actions. Blue circles are the value for w, red crosses the value for v. Also shown are the asymptotic approximations, as presented in the original paper [10] and summarized (often with typos) in textbooks [39]. The strong ($v = \frac{4\alpha^2}{9\pi} - \frac{3}{2}[2\log(2) + c] - \frac{3}{4}$) and weak ($v = 3[1 + 2\alpha(1 - P(w)]/3w)$) coupling approximations for v are green lines, where $C \approx 0.5772$ is the Euler-Mascheroni constant and $P(w) = 2[(w-1)^{\frac{1}{2}} - 1]/w \approx 0.2761$ for $w = 3$. The weak ($w = 3$) and strong ($w = 1$) approximations are purple lines.

and w parameters which scale almost linearly in temperature (Fig. 7 or see Fig. 3 in Ref. [22]). Naïve interpretation of those values as simple harmonic oscillators would suggest infeasible high-frequency oscillations at room temperature, with a strong (almost linear) temperature dependence. It may be possible to disentangle the entropic contribution in this Lagrangian, so calculate the correct temperature dependence of the polaron vibration.

Each of the individual dielectrically coupled phonon modes will be scaled by this factor. The electron-phonon coupling in the Fröhlich model is linear and proportional to the infrared activity of the phonon mode. We can therefore simply plot the expected phonon vibrational spectrum from this model, multiplying the phonon frequencies by the scaling factor w, and directly taking the intensity from the infrared activity.

This rate of vibration is for the ground state of the polaron. The polaron binding energies, indicating where this polaron state is relative to the band edges, are given in Table III. The states between here and the band edges are a continuum from the fully bound state (where k is some factor of v and w) to a fully unbound state (where $k = 0$). We can expect k to linearly decrease as a function of polaron excitation, and so the observed polaron vibrational modes will decrease linearly from these ground-state values to zero at the unbound (band edge) state.

As an example to guide experiment interpretation, we simulate a polaron vibrational measurement. We choose the archetype methylammonium-lead-halide perovskite material. The gamma-point phonon frequencies and infrared activities we take from a previous set of density-functional-theory lattice-dynamic calculations [37].

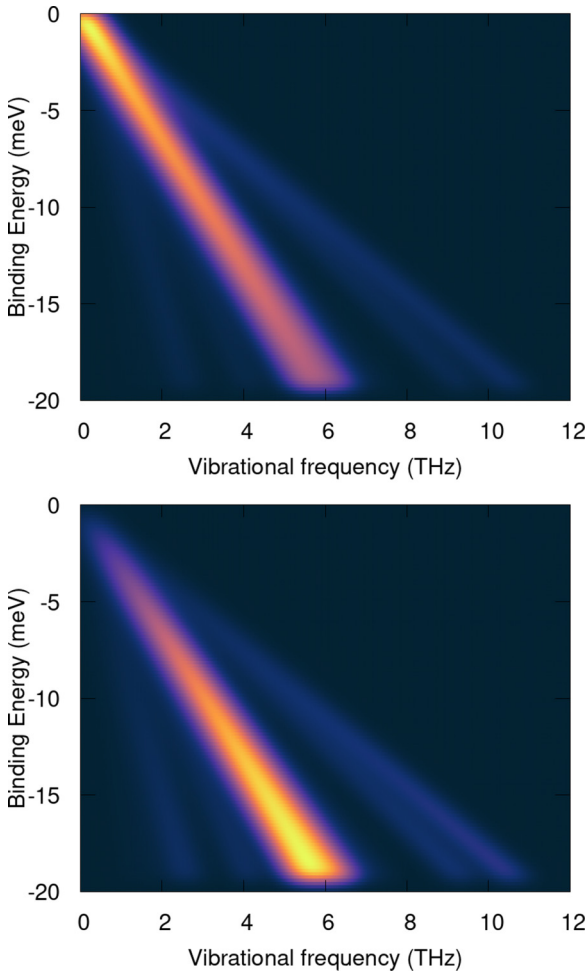

FIG. 17. Simulated $MAPbI_3$ polaron vibrational spectrum. Data consist of the polaron renormalized vibrational modes (Table II), with frequency linear, varied between 0 at the excited band-edge state, to the fully renormalized frequency in the polaron ground state (predicted to lie 19.517 meV below the band edge). These straight lines are weighted by the infrared activity (from Ref. [37]), calculated by projecting Born-effective charges along the gamma-point vibrational modes. These data are then smoothed with a two-dimensional kernel density estimator, with Gaussian widths of 0.5 THz (horizontal) and 0.5 meV (vertical), to provide a guide to how a noiseless low-temperature measurement is predicted to look with this theory. (Top) Constant infrared activity assumed across binding energies. (Bottom) Infrared activity assumed to attenuate to zero as higher-lying polaron excited states are accessed.

We plot these modes as a function of energy below the band edge (Fig. 17). The spring-coupling constant is varied linearly between zero at the band edge to the full ground-state value ($w = 2.68$). This factor scales the vibrational mode.

The resulting finite set of modes and infrared activities are smoothed with a two-dimensional kernel density estimator, with a Gaussian width of 0.5 THz and 0.5 meV. This is intended as a simulation of spectra resolved at low temperature.

VII. DISCUSSION

We have shown that the 60-year-old FHIP [12] mobility theory reproduces much of the "beyond quasiparticle" behavior exhibited in the recent diagrammatic Monte Carlo calculations [26], including violation of the "thermal" Mott-Ioffe-Regel criterion (or Planckian bound [31]) and nonmonotonic temperature dependence.

Additionally, we have extended the Feynman variational approach to the polaron problem to include multiple phonon modes in the effective model action. Compared to Hellwarth and Biaggio's [21] effective mode method, we see additional structure in the frequency-dependent mobility, which has recently become something that can be directly measured [24] in the terahertz regime.

A. Violation of the Mott-Ioffe-Regel criterion versus Planckian bound

The usual MIR criterion puts bounds on transport coefficients of the Boltzmann equations for quasiparticle-mediated transport, where localized wave packets are formed from superpositions of single-particle Bloch states. Beyond these bounds, the mean-free path of a quasiparticle is of order or smaller than its Compton wavelength, where it is no longer possible to form a coherent quasiparticle from superpositions of Bloch states due to the uncertainty in the single-particle state positions.

Violation of the MIR limit is commonly observed in strongly correlated systems at high temperatures and is often used to suggest that transport in these materials is not described by quasiparticle physics. The "thermal" MIR criterion is also a condition on the validity of the Boltzmann description, but is subtly different to the usual MIR criterion as clearly explained by Hartnoll and Mackenzie [31,41] who refer to it instead as a "Planckian bound." Whereas the MIR criterion discerns the ability to form coherent particles from the superposition of Bloch states, the Planckian bound describes the ability of quasiparticles to survive inelastic many-body scattering.

Despite this, here we find that the Feynman variational method, a quasiparticle theory, predicts mobilities outside of the Planckian bound, in good agreement with diagMC mobility predictions. We strongly caution against the use of semiclassical mobility theories using Bloch waves as their charge-carrier wave-function ansatz to model polar materials.

B. Comparison of the FHIP and diagMC mobilities and a note on dissipation

In the Feynman variational theory, we see nonmonotonic temperature dependence in mobility. At strong coupling, there are a range of temperatures where the temperature exponent of the mobility is negative, which begins around $T \simeq \hbar\omega_0$ and ends around some temperature that scales with the Fröhlich coupling parameter α. The latter high-temperature limit marks the transition from strongly coupled polaronic excitations to a thermal electron state [Eq. (35)], which is reached asymptotically at large temperatures. Compared to the diagMC mobility, we need to go to larger α parameters (beyond 8) to start to see a "ski jump" rise in mobility with temperature, whereas in diagMC this is seen already at $\alpha = 6$. Although, we note that our FHIP results lie within the majority of the Monte Carlo error bars.

While the temperature dependence of the FHIP mobility agrees well with the diagMC results, the frequency dependence differs greatly. This has already been investigated [32] and is due to the harmonic nature of the Feynman trial action. The Feynman trial action lacks a dissipative mechanism for the polaron, such that the polaron state described by this model does not lose energy and has an infinite lifetime. The spectral function for this model, $A(\Omega) = -2\,\mathrm{Im}\chi(\Omega)$ (where χ is the memory function), is a series of delta functions. In [32], this is corrected by including additional dissipation processes, whose strength is fixed by an exact sum rule. This was achieved by directly altering the FHIP memory function, such that the resultant spectral function is a series of Gaussian functions. Their resultant frequency-dependent mobility has better agreement with the diagMC mobility.

Another alternative approach to include dissipation may be to extend the trial The Lagrangian in Eq. (53) to incorporate dissipation while maintaining that the resulting trial path integral still be evaluable [42,43]. This would also enable the direct inclusion of anharmonic phonons. Applying these generalized trial actions will be the subject of future work.

C. Numerical evaluation of the memory function

Part of evaluating the FHIP mobility requires a numerical integration in the "memory function" given in Eq. (26). While this is usually done by rotating the contour of the integral [given by Eqs. (32) and (33)] and expanding as a power series of special functions, we found that it is far more computationally efficient to directly evaluate the original (nonrotated) integral, using standard adaptive Gauss-quadrature methods. Part of this investigation leads us to derive power-series expansions for the real and imaginary components of the memory function, which we show in the Appendixes. The expansion for the imaginary component in terms of Bessel-K functions has been produced before in [27], however, we found an expansion for the real component in terms of Bessel-I and Struve-L functions. While we ultimately did not use these expansions in our numeric results presented here, asymptotic evaluation of these forms may be useful for future theoretical analysis or numerical calculations.

D. FHIP initial product state and low-temperature mobility

In Sec. II B, we briefly mentioned that in FHIP [12] they assume a nonphysical initial state, which results in an incorrect low-temperature weak-coupling approximation for the dc mobility with a spurious "$2\beta''$ appearing in the denominator of the mobility,

$$\mu_{\mathrm{FHIP}} = \left(\frac{w}{v}\right)^3 \frac{3e}{2m^*} \frac{\exp(\beta)}{2\beta\alpha\Omega} \exp\left(\frac{v^2 - w^2}{w^2 v}\right). \tag{54}$$

This observation is important for understanding the $3/2\beta$ discrepancy between the low-temperature FHIP dc mobility and Kadanoff's dc mobility [44] derived from the Boltzmann equation

$$\mu_{\mathrm{K}} = \left(\frac{w}{v}\right)^3 \frac{e}{2m^*} \frac{\exp(\beta)}{\alpha\Omega} \exp\left(\frac{v^2 - w^2}{w^2 v}\right). \tag{55}$$

Some have argued that this discrepancy is due to taking the incorrect order of the limits $\Omega \to 0$ and $\alpha \to 0$ [45]. An alternative form of the low-temperature dc mobility was derived by Los [46–48] and Sels [29]. Their mobility results differ by a factor of 3 from Kadonoff and by a factor of 2β from FHIP:

$$\mu_{\mathrm{L}} = \left(\frac{w}{v}\right)^3 \frac{3e}{2m^*} \frac{\exp(\beta)}{\alpha\Omega} \exp\left(\frac{v^2 - w^2}{w^2 v}\right). \tag{56}$$

Sels [29] shows that the difference with Kadonoff is because the relaxation time approximation (neglecting the nonvanishing in-scattering term) used by Kadonoff violates particle number conservation, whereas FHIP does not. However, the FHIP approximation relies on a nonphysical initial state for Feynman's polaron model, as mentioned above. Further, Los [47,48] shows that not using a factorized initial state of the electron-phonon system results in corrections (although small) due to initial correlations being neglected.

In this work we do not use the low-temperature weak-coupling approximate form of the FHIP mobility, instead, we perform a direct numerical integration of the integral in the memory function χ in Eq. (31).

E. Multimodal extension to the Feynman variation approach

We compared the free energy and linear response of the polaron evaluated from the Hellwarth and Biaggio [21] effective phonon mode method to our explicit multiple phonon mode method. Applied to the 15 optical solid-state phonon modes in $MAPbI_3$, we show that our explicit mode method predicts slightly higher mobility for temperatures 0 to 400 K, to a maximum of 20% increase at 100 K. At 300 K we predict electron and hole mobilities of 160 and 112 $\mathrm{cm^2\ V^{-1}\ s^{-1}}$, respectively. This is to be compared to our previous predictions of 133 and 94 $\mathrm{cm^2\ V^{-1}\ s^{-1}}$ for one effective phonon mode evaluated using Hellwarth and Biaggio's [21] B scheme [see Eqs. (52a) and (52b)] of 2.25 THz, as evaluated in our previous work in Ref. [22].

More importantly, we recover considerable structure in the complex conductivity and impedance functions as individual phonon modes are activated. This theory provides a quantitative quantum-mechanical method to predict the structure we proposed from semiclassical reasoning in [49] (see Fig. 10). Towards higher temperatures the effective and explicit methods show the same temperature and frequency dependence: the quantum details are washed out.

F. Future work and outlook

There are many possible extensions of the Feynman polaron approach to increase the accuracy of the approximations and to more accurately model real systems. As discussed, dissipative processes in the trial action would avoid unphysical failures to thermalize and spurious quantum recurrences, most notable in the frequency-dependent mobility. This requires generalizing the trial action. Recently, Ichmoukhamedov and Tempere [43], in applying the variational path-integral approach to the Bogoliubov-Fröhlich Hamiltonian, extended the trial action to a more general form, and also considered higher-order corrections beyond the Jensen-Feynman inequality. While the higher-order corrections are known to be small for the original Fröhlich model [50,51], they may be important for more general electron-phonon interaction Hamiltonians.

Recently, Houtput *et al.* [52] have extended the Fröhlich model to anharmonic phonon modes. They show that anharmonicity further localizes the polaron. As $MAPbI_3$ and other soft polar semiconductors are highly anharmonic, extending the mobility theory of this paper to include anharmonic couplings would be of considerable utility.

Throughout this paper, we have restricted ourselves to a single pair of v and w variational parameters. It is possible to generalize the theory to multiple normal modes in the quasiparticle solution, which allows for richer structure in the mobility theory, and a closer approximation to complex multimode materials.

The FHIP approach [12] is limited to the linear-response regime where the applied field is considered weakly alternating. The linear-response regime is sufficient for most technical applications, but nonlinear effects may be relevant to interpreting pump-probe THz conductivity measurements. The nonlinear extensions [53,54] of FHIP offer a theoretical route to add this in the future.

Open-source Julia [55] codes implementing these methods are available as a repository on GitHub [56].

ACKNOWLEDGMENTS

We thank A. Mishchenko for providing their raw diagrammatic Monte Carlo data [26] for coplotting and for useful discussions. We thank S. Ciuchi and the anonymous reviewer for critically reading an earlier version of this manuscript. B.A.A.M. is supported by an EPSRC Doctoral Training Award (Grant No. 2446070). J.M.F. is supported by a Royal Society University Research Fellowship (Grant No. URF-R1-191292). This work used the Imperial College Research Computing Service [57]. We acknowledge UK's HEC Materials Chemistry Consortium, which is funded by EPSRC (Grant No. EP/R029431), this work used the ARCHER2 UK National Supercomputing Service.

APPENDIX A: CONTOUR INTEGRATION OF THE MEMORY FUNCTION

Following Devreese *et al.* [27] we derived infinite-power-series expansions of the real and imaginary components of Eq. (26) [or Eq. (35) in Ref. [12]] in terms of Bessel and Struve special functions, and hypergeometric functions. The practical computational implementation of these expansions was made difficult by the very high precision required on the special functions to make the expansions converge. Using arbitrary precision numerics, a partially working implementation was developed, but it was discovered that direct numeric integration of Eq. (26) could achieve the same result with less computation time and less complex code.

We start by changing the contour of the memory function as done in Ref. [12]. The memory function for the polaron is defined to linear order in Ref. [15] as $\Sigma(\Omega) = \chi^*(\Omega)/\Omega$, where

$$\chi(\Omega) = \int_0^\infty [1 - e^{i\Omega u}]\mathrm{Im}S(u)\, du \tag{A1}$$

is the

$$S(u) = \frac{2\alpha}{3\sqrt{\pi}}[D(u)]^{-\frac{3}{2}}\left(e^{iu} + \frac{2}{e^\beta - 1}\cos(u)\right) \tag{A2}$$

and

$$D(u) = \frac{w^2}{\beta v^2}\{a^2 - \beta^2/4 - b\cos(vu)\cosh(v\beta/2) + u^2 - i[b\sin(vu)\sinh(v\beta/2) + u\beta]\}, \tag{A3}$$

with $R \equiv (v^2 - w^2)/(w^2 v)$, $a^2 = \beta^2/4 + R\beta\coth(\beta v/2)$ and $b = R\beta\ /\ \sinh(\beta v/2)$, which are the same as Eqs. (47b) in Ref. [12].

Solving for the real and imaginary parts of $\Sigma(\Omega)$ gives the real and imaginary parts of $\chi(\Omega)$:

$$\mathrm{Re}\,\chi(\Omega) = \int_0^\infty [1 - \cos(\Omega u)]\mathrm{Im}S(u)\, du, \tag{A4a}$$

$$\mathrm{Im}\,\chi(\Omega) = \int_0^\infty \sin(\Omega u)\,\mathrm{Im}S(u)\, du. \tag{A4b}$$

As both $[1 - \cos(\Omega u)]$ and $\sin(\Omega)$ are real we can take Im outside the integral,

$$\mathrm{Re}\,\chi(\Omega) = \mathrm{Im}\int_0^\infty [1 - \cos(\Omega u)]S(u)\, du, \tag{A5a}$$

$$\mathrm{Im}\,\chi(\Omega) = \mathrm{Im}\int_0^\infty \sin(\Omega u)\, S(u)\, du. \tag{A5b}$$

Now we promote $u \in \mathbb{R}$ to a complex variable $u = x + iy \in \mathbb{C}$. The integrals then become integrals on the complex plane,

$$\mathrm{Re}\chi(\Omega) = \mathrm{Im}\int_\Gamma [1 - \cos(\Omega x)\cosh(\Omega y) + i\sin(\Omega x)\sinh(\Omega y)]S(x + iy)\, du, \tag{A6a}$$

$$\mathrm{Im}\chi(\Omega) = \mathrm{Im}\int_\Gamma [\sin(\Omega x)\cosh(\Omega y) + i\cos(\Omega x)\sinh(\Omega y)]S(x + iy)\, du, \tag{A6b}$$

where Γ is our contour of integration. To motivate a choice of contour, let us consider the form of $D(x + iy)$ and $S(x + iy)$:

$$D(x + iy) = \frac{w^2}{\beta v^2}\{[a^2 - \beta^2/4 - b\cos(vx)\cosh[v(y - \beta/2)] + x^2 + y(\beta - y)] + i\{b\sin(vx)\sinh \times [v(y - \beta/2)] + 2x(y - \beta/2)\}\}, \tag{A7}$$

$$S(x + iy) = \frac{2\alpha}{3\sqrt{\pi}}\frac{\cos[x + i(y - \beta/2)]}{\sinh(\beta/2)[D(x + iy)]^{\frac{3}{2}}}. \tag{A8}$$

Now we notice that $D(x + iy)$ and $S(x + iy)$ are trivially real when $y = \beta/2$. This gives the results

$$D(x + i\beta/2) = \frac{w^2}{\beta v^2}[x^2 + a^2 - b\cos(vx)] \in \mathbb{R}, \tag{A9}$$

$$S(x + i\beta/2) = \frac{2\alpha}{3\sqrt{\pi}}\frac{\beta^{\frac{3}{2}}}{\sinh(\beta/2)}\left(\frac{v}{w}\right)^3\frac{\cos(x)}{\times [x^2 + a^2 - b\cos(vx)]^{\frac{3}{2}}} \in \mathbb{R}. \tag{A10}$$

From this, we choose to integrate over the contours $\Gamma_1 \in (\infty + 0i, 0 + 0i] \to \Gamma_2 \in [0 + i0, 0 + i\beta/2] \to \Gamma_3 \in [0 + i\beta/2, \infty + i\beta/2) \to \Gamma_4 \in (\infty + i\beta/2, \infty + 0i)$ as shown in Fig. 18. Since the integrands in Eqs. (A6a) and (A6b) are analytic in this region, this closed contour integral will be zero. [There is a pole in $\mathrm{Im}S(x + iy)$ at $0 + i0$, but this is canceled by the zero of the elementary and trigonometric functions in front of it at this point.] The closing piece of the contour lies at $x \to \infty$ and can be neglected as $S(x + iy) \to 0$ in this limit.

Thus, for the real part of $\chi(\Omega)$ we have

$$\begin{aligned}\int_0^\infty &[1 - \cos(\Omega x)]S(x)\,dx \\ &= \int_0^{\beta/2} [1 - \cosh(\Omega y)]S(iy)\,d(iy) \\ &\quad + \int_0^\infty \left[1 - \cos(\Omega x)\cosh\left(\frac{\Omega\beta}{2}\right) + i\sin(\Omega x)\right. \\ &\quad \left.\times \sinh\left(\frac{\Omega\beta}{2}\right)\right] S\left(x + \frac{i\beta}{2}\right) dx, \end{aligned} \tag{A11}$$

and for the imaginary part of $\chi(\Omega)$ we have

$$\begin{aligned}\int_0^\infty &\sin(\Omega x)S(x)\,dx \\ &= i\int_0^{\beta/2} \sinh(\Omega y)S(iy)\,d(iy) \\ &\quad + \int_0^\infty \left[\sin(\Omega x)\cosh\left(\frac{\Omega\beta}{2}\right)\right. \\ &\quad \left. + i\cos(\Omega x)\sinh\left(\frac{\Omega\beta}{2}\right)\right] S\left(x + \frac{i\beta}{2}\right) dx. \end{aligned} \tag{A12}$$

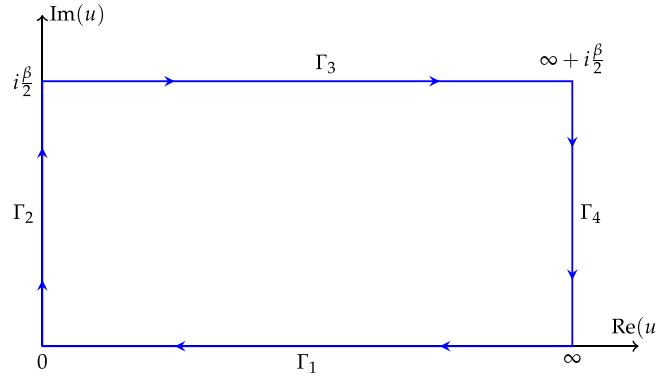

FIG. 18. The complex contour chosen to transform the integral in Eq. (A1). No singularities lie within the closed contour so the contour integral is zero.

We can now see more clearly why we choose to integrate at $y = \beta/2$. Since $S(x + i\beta/2)$ is real, acting Im on these integrals will cancel the second integral in the contour integral for $\mathrm{Im}\chi(\Omega)$ (which is entirely real), and the third integral for both $\mathrm{Re}\chi(\Omega)$ and $\mathrm{Im}\chi(\Omega)$ is simplified due to the absence of any cross terms that would have resulted for other values of y as $S(x + iy)$ would have been complex. To see that the second integral for $\mathrm{Im}\chi(\Omega)$ is real, we need to see if $S(iy)$ is real. First, we look at $D(iy)$, which is given by

$$\begin{aligned} D(iy) = \frac{w^2}{\beta v^2}\Bigg[a^2 - \frac{\beta^2}{4} + y(\beta - y) - b \\ \times \cosh\left(vy - \frac{\beta v}{2}\right)\Bigg] \in \mathbb{R}, \end{aligned} \tag{A13}$$

and then $S(iy)$ is given by

$$S(iy) = \frac{2\alpha}{3\sqrt{\pi}} \frac{\beta^{3/2}}{\sinh(\beta/2)} \left(\frac{v}{w}\right)^3 \frac{\cosh(y - \beta/2)}{\{a^2 - \beta^2/4 + y(\beta - y) - b\cosh[v(y - \beta/2)]\}^{3/2}} \in \mathbb{R}, \tag{A14}$$

so $S(iy)$ is indeed real. Since the second integral for $\mathrm{Im}\chi(\Omega)$ has two complex i and $S(iy)$ is real, the whole integral is entirely real and so it does not contribute to $\mathrm{Im}\chi(\Omega)$. Unfortunately, $\mathrm{Re}\chi(\Omega)$ does not simplify as nicely as $\mathrm{Im}\chi(\Omega)$ because the second integral is imaginary and so is still present after taking only the imaginary parts. Nonetheless, for $\mathrm{Re}\chi(\Omega)$ we get

$$\begin{aligned}\mathrm{Re}\chi(\Omega) = \mathrm{Im}\int_0^\infty [1 - \cos(\Omega x)]S(x)\,dx = \frac{2\alpha}{3\sqrt{\pi}} \frac{\beta^{3/2}}{\sinh(\beta/2)} \left(\frac{v}{w}\right)^3 \Bigg\{\sinh\left(\frac{\Omega\beta}{2}\right) \int_0^\infty \frac{\sin(\Omega x)\cos(x)\,dx}{[x^2 + a^2 - b\cos(vx)]^{3/2}} \\ + \int_0^{\beta/2} \frac{[1 - \cosh(\Omega x)]\cosh(x - \beta/2)\,dx}{\{a^2 - \beta^2/4 + x(\beta - x) - b\cosh[v(x - \beta/2)]\}^{3/2}}\Bigg\}, \end{aligned} \tag{A15}$$

and for $\mathrm{Im}\chi(\Omega)$ we get

$$\mathrm{Im}\chi(\Omega) = \mathrm{Im}\int_0^\infty \sin(\Omega x)S(x)\,dx = \frac{2\alpha}{3\sqrt{\pi}} \frac{\beta^{3/2}\sinh(\Omega\beta/2)}{\sinh(\beta/2)} \left(\frac{v}{w}\right)^3 \int_0^\infty \frac{\cos(\Omega x)\cos(x)\,dx}{[x^2 + a^2 - b\cos(vx)]^{3/2}}. \tag{A16}$$

APPENDIX B: IMχ EXPANSION IN BESSEL-K FUNCTIONS

In Devreese *et al.* Ref. [27] the integral in Eq. (A16) is expanded in an infinite sum of modified Bessel functions of the second kind. Here we follow the same procedure and arrive at the same result, but provide detailed workings. Specifically, we are interested in solving the integral

$$\int_0^\infty \frac{\cos(\Omega x)\cos(x)\,dx}{[x^2 + a^2 - b\cos(vx)]^{3/2}}. \tag{B1}$$

We start by noticing that

$$\left|\frac{b\cos(vx)}{x^2+a^2}\right| < 1 \quad \text{if } v > 0 \text{ and } \beta > 0, \tag{B2}$$

so we can do a binomial expansion of the denominator

$$\begin{aligned}\int_0^\infty \frac{\cos(\Omega x)\cos(x)}{(x^2+a^2)^{3/2}}\left[1-\frac{b\cos(vx)}{x^2+a^2}\right]^{-3/2}dx &= \int_0^\infty dx\,\frac{\cos(\Omega x)\cos(x)}{(x^2+a^2)^{3/2}}\sum_{n=0}^\infty \binom{-3/2}{n}\frac{(-b)^n\cos^n(vx)}{(x^2+a^2)^n}dx \\ &= \sum_{n=0}^\infty \binom{-3/2}{n}(-b)^n\int_0^\infty \frac{\cos(\Omega x)\cos(x)\cos^n(vx)}{(x^2+a^2)^{n+3/2}}\,dx,\end{aligned} \tag{B3}$$

where $\binom{-3/2}{n}$ is a binomial coefficient. Next, we expand $\cos^n(vx)$ using the power-reduction formula

$$\cos^n(vx) = \frac{2}{2^n}\sum_{k=0}^{\lfloor\frac{n-1}{2}\rfloor}\binom{n}{k}\cos[(n-2k)vx] + \frac{(1-n\bmod 2)}{2^n}\binom{n}{\frac{n}{2}}, \tag{B4}$$

where the second term comes from even n contributions only. Substituting this into our integral gives

$$\sum_{n=0}^\infty \binom{-3/2}{n}\left(-\frac{b}{2}\right)^n\left[2\sum_{k=0}^{\lfloor\frac{n-1}{2}\rfloor}\binom{n}{k}\int_0^\infty \frac{\cos(\Omega x)\cos(x)\cos[(n-2k)vx]}{(x^2+a^2)^{n+3/2}}\,dx + (1-n\bmod 2)\binom{n}{\frac{n}{2}}\int_0^\infty \frac{\cos(\Omega x)\cos(x)}{(x^2+a^2)^{n+3/2}}\,dx\right]. \tag{B5}$$

We can now combine the cosines inside of the integrals into sums of single cosines using

$$\begin{aligned}\cos(\Omega x)\cos(x)\cos[vx(n-2k)] &= \frac{1}{4}\{\cos(x\{\Omega+1+v(n-2k)]\} + \cos\{x[\Omega-1+v(n-2k)]\} \\ &\quad + \cos\{x[\Omega+1-v(n-2k)]\} + \cos\{x[\Omega-1-v(n-2k)]\}\} \\ &\equiv \frac{1}{4}\sum_{z_4}\cos\left(xz_{k,4}^n\right),\end{aligned} \tag{B6}$$

where for brevity we have defined $z_{k,4}^n \in \{\Omega+1+v(n-2k),\ \Omega-1+v(n-2k),\ \Omega+1-v(n-2k),\ \Omega-1-v(n-2k)\}$. Likewise,

$$\cos(\Omega x)\cos(x) = \frac{1}{2}\left\{\cos[x(\Omega+1)] + \cos[x(\Omega-1)]\right\} \equiv \frac{1}{2}\sum_{z_2}\cos(xz_2), \tag{B7}$$

where for brevity we have defined $z_2 \in \{\Omega+1,\ \Omega-1\}$. Substituting these into our expansion gives

$$\sum_{n=0}^\infty \binom{-3/2}{n}\left(-\frac{b}{2}\right)^n\left[2\sum_{k=0}^{\lfloor\frac{n-1}{2}\rfloor}\binom{n}{k}\sum_{z_4}\int_0^\infty \frac{\cos\left[xz_{k,4}^n(\Omega)\right]}{(x^2+a^2)^{n+3/2}}\,dx + (1-n\bmod 2)\binom{n}{\frac{n}{2}}\sum_{z_2}\int_0^\infty \frac{\cos[xz_2(\Omega)]}{(x^2+a^2)^{n+3/2}}\,dx\right]. \tag{B8}$$

We now have a lot of integrals of the form

$$\int_0^\infty \frac{\cos(xz)}{(x^2+a^2)^{n+3/2}}\,dx, \tag{B9}$$

which is an integral representation of modified Bessel functions of the second kind,

$$\begin{aligned}\int_0^\infty \frac{\cos(xz)\,dx}{(x^2+a^2)^{n+3/2}} &= \frac{\sqrt{\pi}}{\Gamma(n+3/2)}K_{n+1}(|z|a)\left|\frac{z}{2a}\right|^{n+1} \\ &\equiv B_n(z).\end{aligned} \tag{B10}$$

Thus, overall we can expand $\mathrm{Im}\chi(\Omega)$ in a series of these Bessel functions,

$$\mathrm{Im}\chi(\Omega) = \frac{2\alpha\beta^{\frac{3}{2}}}{3\sqrt{\pi}}\frac{\sinh\left(\frac{\Omega\beta}{2}\right)}{\sinh\left(\frac{\beta}{2}\right)}\left(\frac{v}{w}\right)^3\sum_{n=0}^\infty\binom{-\frac{3}{2}}{n}\left(-\frac{b}{2}\right)^n\left[\sum_{k=0}^{\lfloor\frac{n-1}{2}\rfloor}\binom{n}{k}\sum_{z_4}B_n\left[z_{k,4}^n(\Omega)\right] + (1-n\bmod 2)\binom{n}{\frac{n}{2}}\sum_{z_2}B_n[z_2(\Omega)]\right], \tag{B11}$$

where $a^2 = \beta^2/4 + R\beta\coth(\beta v/2)$, $b = R\beta/\sinh(\beta v/2)$, and $R = (v^2-w^2)/(w^2v)$. Also, $z_{k,4}^n(\Omega) \in \{\Omega+1+v(n-2k),\ \Omega-1+v(n-2k),\ \Omega+1-v(n-2k),\ \Omega-1-v(n-2k)\}$ and $z_2(\Omega) \in \{\Omega+1,\ \Omega-1\}$.

APPENDIX C: REχ EXPANSION IN BESSEL-I, STRUVE-L, AND ${}_1F_2$ HYPERGEOMETRIC FUNCTIONS

Motivated by the expansion of Im$\chi(\Omega)$ in Devreese *et al.* [27] we provide a similar expansion for Re$\chi(\Omega)$. We follow a similar procedure as for Im$\chi(\Omega)$ and notice that our efforts focus on solving the integrals

$$\int_0^\infty \frac{\sin(\Omega x)\cos(x)\,dx}{[x^2+a^2-b\cos(vx)]^{3/2}}, \tag{C1}$$

$$\int_0^{\beta/2} \frac{[1-\cosh(\Omega x)]\cosh(x-\beta/2)\,dx}{\{a^2-\beta^2/4+x(\beta-x)-b\cosh[v(x-\beta/2)]\}^{3/2}}. \tag{C2}$$

The first integral is very similar to Eq. (B1), just with a cosine swapped out for a sine. Following a similar procedure as for Eq. (B1) gives

$$\int_0^\infty \frac{\sin(\Omega x)\cos(x)\,dx}{[x^2+a^2-b\cos(vx)]^{3/2}} = \sum_{n=0}^\infty \binom{-3/2}{n}\left(-\frac{b}{2}\right)^n \left[2\sum_{k=0}^{\lfloor\frac{n-1}{2}\rfloor}\binom{n}{k}\sum_{z_4}\int_0^\infty \frac{\sin\left[xz_{k,4}^n(\Omega)\right]}{(x^2+a^2)^{n+3/2}}\,dx + (1-n\bmod 2)\binom{n}{\frac{n}{2}} \times \sum_{z_2}\int_0^\infty \frac{\sin[xz_2(\Omega)]}{(x^2+a^2)^{n+3/2}}\,dx\right], \tag{C3}$$

where we now look for any special functions for which

$$\int_0^\infty \frac{\sin(xz)}{(x^2+a^2)^{n+3/2}}\,dx \tag{C4}$$

is the integral representation. We found that

$$\int_0^\infty \frac{\sin(xz)}{(x^2+a^2)^{n+3/2}}\,dx = \frac{\sqrt{\pi}}{2}\frac{\Gamma\left(-\frac{1}{2}-n\right)\operatorname{sgn}(z)|z|^{n+1}}{(2a)^{n+1}}[I_{n+1}(|z|a)-\mathbf{L}_{-(n+1)}(|z|a)] \equiv J_n(z) \tag{C5}$$

for $n \geqslant 0$ and $a \geqslant 0$. Here sgn(x) is the signum function, $I_n(x)$ is the modified Bessel function of the first kind, $\mathbf{L}_n(x)$ is the modified Struve function. Therefore, for Re$\chi(\Omega)$ we have

$$\mathrm{Re}\chi(\Omega) = \frac{2\alpha\beta^{3/2}}{3\sqrt{\pi}}\frac{\sinh\left(\frac{\Omega\beta}{2}\right)}{\sinh(\beta/2)}\left(\frac{v}{w}\right)^3\left\{\sum_{n=0}^\infty\binom{-\frac{3}{2}}{n}\left(\frac{b}{2}\right)^n\left[\sum_{k=0}^{\lfloor\frac{n-1}{2}\rfloor}\binom{n}{k}\sum_{z_4}J_n[z_{k,4}^n(\Omega)] + (1-n\bmod 2)\binom{n}{\frac{n}{2}}\sum_{z_2}J_n[z_2(\Omega)]\right]\right\} + \frac{2\alpha}{3\sqrt{\pi}}\frac{\beta^{3/2}}{\sinh(\beta/2)}\left(\frac{v}{w}\right)^3\int_0^{\beta/2}\frac{[1-\cosh(\Omega x)]\cosh(x-\beta/2)\,dx}{\{a^2-\beta^2/4+x(\beta-x)-b\,\cosh[v(x-\beta/2)]\}^{3/2}}, \tag{C6}$$

where a, b, z_4, and z_2 are the same as before.

Expanding the second integral with the hyperbolic integrand is more complicated. We start by doing a change of variables $x \to (1-x)\beta/2$ to transform the denominator into a similar form as before and to change the limits to [0, 1]:

$$\int_0^{\beta/2}\frac{[1-\cosh(\Omega x)]\cosh(x-\beta/2)\,dx}{\{a^2-\beta^2/4+x(\beta-x)-b\,\cosh[v(x-\beta/2)]\}^{3/2}} \longrightarrow \frac{\beta}{2}\int_0^1\frac{[1-\cosh(\Omega\beta[1-x]/2)]\cosh(\beta x/2)dx}{[a^2-(\beta x/2)^2-b\cosh(\beta vx/2)]^{3/2}}. \tag{C7}$$

Now we see that for $x \in [0, 1]$

$$\left|\frac{b\,\cosh(v\beta x/2)}{a^2-(\beta x/2)^2}\right| < 1 \quad \text{if } v > 0 \text{ and } \beta > 0 \tag{C8}$$

so we can do a binomial expansion of the denominator as before:

$$\sum_{n=0}^\infty\binom{-\frac{3}{2}}{n}\left(\frac{2}{\beta}\right)^{2n+2}(-b)^n\int_0^1\frac{[1-\cosh(\Omega\beta[1-x]/2)]\cosh(\beta x/2)\cosh^n(v\beta x/2)}{[(2a/\beta)^2-x^2]^{n+3/2}}dx. \tag{C9}$$

Then we do another binomial expansion of the remaining denominator:

$$\sum_{n=0}^\infty\binom{-\frac{3}{2}}{n}\left(\frac{2}{\beta}\right)^{2n+2}(-b)^n\sum_{m=0}^\infty\binom{-n-\frac{3}{2}}{m}(-1)^m\left(\frac{\beta}{2a}\right)^{2n+2m+3} \times\int_0^1\left[1-\cosh\left(\frac{\Omega\beta[1-x]}{2}\right)\right]\cosh\left(\frac{\beta x}{2}\right)\cosh^n\left(\frac{v\beta x}{2}\right)x^{2m}dx. \tag{C10}$$

We can then expand the product of hyperbolic cosines in the integrand

$$\sum_{n=0}^{\infty}\binom{-\frac{3}{2}}{n}\left(\frac{2}{\beta}\right)^{2n+2}(-b)^n\sum_{m=0}^{\infty}\binom{-n-\frac{3}{2}}{m}(-1)^m\left(\frac{\beta}{2a}\right)^{2n+2m+3}\frac{1}{2^n}$$
$$\times\left\{\binom{n}{\frac{n}{2}}(1-n\bmod 2)\left[\int_0^1\frac{\cosh\left(\frac{\beta z_1 x}{2}\right)}{x^{-2m}}dx-\frac{1}{2}\sum_{z_2}\left(\cosh\left(\frac{\Omega\beta}{2}\right)\int_0^1\frac{\cosh\left(\frac{\beta z_2 x}{2}\right)}{x^{-2m}}dx-\sinh\left(\frac{\Omega\beta}{2}\right)\int_0^1\frac{\sinh\left(\frac{\beta z_2 x}{2}\right)}{x^{-2m}}dx\right)\right]\right.$$
$$\left.+\sum_{k=0}^{\lfloor\frac{n-1}{2}\rfloor}\binom{n}{k}\left[\sum_{z_3}\int_0^1\frac{\cosh\left(\frac{\Omega\beta z_3 x}{2}\right)}{x^{-2m}}dx-\frac{1}{2}\sum_{z_4}\left(\cosh\left(\frac{\Omega\beta}{2}\right)\int_0^1\frac{\cosh\left(\frac{\Omega\beta z_4 x}{2}\right)}{x^{-2m}}dx-\sinh\left(\frac{\Omega\beta}{2}\right)\int_0^1\frac{\sinh\left(\frac{\Omega\beta z_4 x}{2}\right)}{x^{-2m}}dx\right)\right]\right\},\tag{C11}$$

where $z_1=1$, $z_2(\Omega)\in\{\Omega+1,\ \Omega-1\}$, $z^n_{k,3}\in\{1+v(n-2k),\ 1-v(n-2k)\}$, and $z^n_{k,4}(\Omega)\in\{\Omega+1+v(n-2k),\ \Omega-1+v(n-2k),\ \Omega+1-v(n-2k),\ \Omega-1-v(n-2k)\}$.

Now we have two integrals of the forms

$$\int_0^1\cosh(zx)x^{2m}dx,\quad \int_0^1\sinh(zx)x^{2m}dx,\tag{C12}$$

which are the integral forms of the generalized hypergeometric functions

$$\int_0^1\cosh(zx)x^{2m}dx={}_1F_2\left[\begin{matrix}m+\frac{1}{2}\\ \frac{1}{2}\ \ m+\frac{3}{2}\end{matrix};\frac{z^2}{4}\right]=\sum_{t=0}^{\infty}\frac{z^{2t}}{(2t+2m+1)(2t)!},\quad m>-\frac{1}{2}\tag{C13a}$$

$$\int_0^1\sinh(zx)x^{2m}dx=\frac{z}{2m+2}{}_1F_2\left[\begin{matrix}m+1\\ \frac{3}{2}\ \ m+2\end{matrix};\frac{z^2}{4}\right]=\sum_{t=0}^{\infty}\frac{z^{2t+1}}{(2t+2m+2)(2t+1)!},\quad m>-1.\tag{C13b}$$

For brevity, we will define

$${}_1F_2^c(z)\equiv{}_1F_2\left[\begin{matrix}m+\frac{1}{2}\\ \frac{1}{2}\ \ m+\frac{3}{2}\end{matrix};\frac{\beta^2z^2}{16}\right]=\sum_{t=0}^{\infty}\frac{(\beta z/2)^{2t}}{(2t+2m+1)(2t)!},\tag{C14a}$$

$${}_1F_2^s(z)\equiv\frac{\beta z}{4m+4}{}_1F_2\left[\begin{matrix}m+1\\ \frac{3}{2}\ \ m+2\end{matrix};\frac{\beta^2z^2}{16}\right]=\sum_{t=0}^{\infty}\frac{(\beta z/2)^{2t+1}}{(2t+2m+2)(2t+1)!}\tag{C14b}$$

so that Eq. (C11) becomes

$$\sum_{n=0}^{\infty}\binom{-\frac{3}{2}}{n}\left(\frac{2}{\beta}\right)^{2n+2}(-b)^n\sum_{m=0}^{\infty}\binom{-n-\frac{3}{2}}{m}(-1)^m\left(\frac{\beta}{2a}\right)^{2n+2m+3}\frac{1}{2^n}$$
$$\times\left\{\binom{n}{\frac{n}{2}}(1-n\bmod 2)\left[{}_1F_2^c(z_1)-\frac{1}{2}\sum_{z_2}\left[\cosh\left(\frac{\Omega\beta}{2}\right){}_1F_2^c(z_2)-\sinh\left(\frac{\Omega\beta}{2}\right){}_1F_2^s(z_2)\right]\right]\right.$$
$$\left.+\sum_{k=0}^{\lfloor\frac{n-1}{2}\rfloor}\binom{n}{k}\left[\sum_{z_3}{}_1F_2^c(z_3)-\frac{1}{2}\sum_{z_4}\left[\cosh\left(\frac{\Omega\beta}{2}\right){}_1F_2^c(z_4)-\sinh\left(\frac{\Omega\beta}{2}\right){}_1F_2^s(z_4)\right]\right]\right\}\tag{C15}$$

which we can reduce further by defining

$$M_n^{c/s}(z)\equiv\sum_{m=0}^{\infty}\binom{-n-\frac{3}{2}}{m}(-1)^m a^{-2(n+m+1)}\left(\frac{\beta}{2}\right)^{2m+1}{}_1F_2^{c/s}(z)\tag{C16}$$

to give

$$\sum_{n=0}^{\infty}\binom{-\frac{3}{2}}{n}\left(\frac{-b}{2}\right)^n\left\{\binom{n}{\frac{n}{2}}(1-n\bmod 2)\left[M_n^c(z_1)-\frac{1}{2}\sum_{z_2}\left[\cosh\left(\frac{\Omega\beta}{2}\right)M_n^c(z_2)-\sinh\left(\frac{\Omega\beta}{2}\right)M_n^s(z_2)\right]\right]\right.$$
$$\left.+\sum_{k=0}^{\lfloor\frac{n-1}{2}\rfloor}\binom{n}{k}\left[\sum_{z_3}M_n^c(z_3)-\frac{1}{2}\sum_{z_4}\left[\cosh\left(\frac{\Omega\beta}{2}\right)M_n^c(z_4)-\sinh\left(\frac{\Omega\beta}{2}\right)M_n^s(z_4)\right]\right]\right\}. \tag{C17}$$

Combining this with the rest of $\mathrm{Re}\chi(\Omega)$ gives

$$\mathrm{Re}\chi(\Omega)=\frac{2\alpha\beta^{3/2}v^3}{3\sqrt{\pi}w^3\sinh(\beta/2)}\sum_{n=0}^{\infty}\binom{-\frac{3}{2}}{n}\left(-\frac{b}{2}\right)^n$$
$$\times\left\{\binom{n}{\frac{n}{2}}(1-n\bmod 2)\left[M_n^c(1)+\frac{1}{2}\sum_{z_2}\left[\sinh\left(\frac{\Omega\beta}{2}\right)\{M_n^s[z_2(\Omega)]+J_n[z_2(\Omega)]\}-\cosh\left(\frac{\Omega\beta}{2}\right)M_n^c[z_2(\Omega)]\right]\right]\right.$$
$$\left.+\sum_{k=0}^{\lfloor\frac{n-1}{2}\rfloor}\binom{n}{k}\left[\sum_{z_3}M_n^c(z_{k,3}^n)+\frac{1}{2}\sum_{z_4}\left[\sinh\left(\frac{\Omega\beta}{2}\right)[M_n^s[z_{k,4}^n(\Omega)]+J_n[z_{k,4}^n(\Omega)]]-\cosh\left(\frac{\Omega\beta}{2}\right)M_n^s[z_{k,4}^n(\Omega)]\right]\right]\right\}. \tag{C18}$$

So, altogether we have the expansion for the memory function

$$\chi(\Omega)=\frac{2\alpha\beta^{3/2}v^3}{3\sqrt{\pi}w^3\sinh(\beta/2)}\sum_{n=0}^{\infty}\binom{-\frac{3}{2}}{n}\left(-\frac{b}{2}\right)^n$$
$$\times\left\{\binom{n}{\frac{n}{2}}(1-n\bmod 2)\left[M_n^c(1)+\frac{1}{2}\sum_{z_2}\left[\sinh\left(\frac{\Omega\beta}{2}\right)[M_n^s(z_2)+J_n(z_2)+iB_n(z_2)]-\cosh\left(\frac{\Omega\beta}{2}\right)M_n^c[z_2(\Omega)]\right]\right]\right.$$
$$\left.+\sum_{k=0}^{\lfloor\frac{n-1}{2}\rfloor}\binom{n}{k}\left[\sum_{z_3}M_n^c(z_{k,3}^n)+\frac{1}{2}\sum_{z_4}\left[\sinh\left(\frac{\Omega\beta}{2}\right)[M_n^s(z_{k,4}^n)+J_n(z_{k,4}^n)+iB_n(z_{k,4}^n)]-\cosh\left(\frac{\Omega\beta}{2}\right)M_n^s(z_{k,4}^n)\right]\right]\right\}. \tag{C19}$$

[1] T. Holstein, Studies of polaron motion, Ann. Phys. **8**, 343 (1959).

[2] I. Lang and Y. A. Firsov, Kinetic theory of semiconductors with low mobility, Zh. Eksp. Teor. Fiz. **43**, 1843 (1963) [Sov. Phys.–JETP **16**, 1301 (1963)].

[3] I. Lang and Y. A. Firsov, Mobility of small-radius polarons at low temperatures, Zh. Eksp. Teor. Fiz. **45**, 378 (1964) [Sov. Phys.–JETP **18**, 262 (1964)].

[4] D. Emin, Optical properties of large and small polarons and bipolarons, Phys. Rev. B **48**, 13691 (1993).

[5] A. S. Alexandrov and P. E. Kornilovitch, Mobile Small Polaron, Phys. Rev. Lett. **82**, 807 (1999).

[6] W. H. Sio, C. Verdi, S. Poncé, and F. Giustino, Polarons from First Principles, without Supercells, Phys. Rev. Lett. **122**, 246403 (2019).

[7] C. Franchini, M. Reticcioli, M. Setvin, and U. Diebold, Polarons in materials, Nat. Rev. Mater. **6**, 560 (2021).

[8] H. Fröhlich, Electrons in lattice fields, Adv. Phys. **3**, 325 (1954).

[9] F. Giustino, Electron-phonon interactions from first principles, Rev. Mod. Phys. **89**, 15003 (2017).

[10] R. P. Feynman, Slow electrons in a polar crystal, Phys. Rev. **97**, 660 (1955).

[11] T. Hahn, S. Klimin, J. Tempere, J. T. Devreese, and C. Franchini, Diagrammatic Monte Carlo study of fröhlich polaron dispersion in two and three dimensions, Phys. Rev. B **97**, 134305 (2018).

[12] R. P. Feynman, R. W. Hellwarth, C. K. Iddings, and P. M. Platzman, Mobility of slow electrons in a polar crystal, Phys. Rev. **127**, 1004 (1962).

[13] F. M. Peeters and J. T. Devreese, Nonlinear conductivity in polar semiconductors: Alternative derivation of the Thornber-Feynman theory, Phys. Rev. B **23**, 1936 (1981).

[14] F. M. Peeters and J. T. Devreese, Impedance function of large polarons: An alternative derivation of the Feynman-Hellwarth-Iddings-Platzman theory, Phys. Rev. B **28**, 6051 (1983).

[15] F. M. Peeters and J. T. Devreese, Theory of polaron mobility, *Solid State Physics* (Elsevier, Amsterdam, 1984), pp. 81–133.

[16] F. M. Peeters and J. T. Devreese, Magneto-optical absorption of polarons, Phys. Rev. B **34**, 7246 (1986).

[17] Y. Osaka, Polaron state at a finite temperature, Prog. Theor. Phys. **22**, 437 (1959).

[18] D. Castrigiano and N. Kokiantonis, Classical paths for a quadratic action with memory and exact evaluation of the path integral, Phys. Lett. A **96**, 55 (1983).

[19] D. Castrigiano, N. Kokiantonis, and H. Stierstorfer, Free energy and effective mass of the polaron at finite temperatures, Phys. Lett. A **104**, 364 (1984).

[20] M. Saitoh, Theory of a polaron at finite temperatures, J. Phys. Soc. Jpn. **49**, 878 (1980).

[21] R. W. Hellwarth and I. Biaggio, Mobility of an electron in a multimode polar lattice, Phys. Rev. B **60**, 299 (1999).

[22] J. M. Frost, Calculating polaron mobility in halide perovskites, Phys. Rev. B **96**, 195202 (2017).

[23] J. M. Frost, PolaronMobility.jl: Implementation of the Feynman variational polaron model, J. Open Source Software **3**, 566 (2018).

[24] X. Zheng, T. R. Hopper, A. Gorodetsky, M. Maimaris, W. Xu, B. A. A. Martin, J. M. Frost, and A. A. Bakulin, Multipulse terahertz spectroscopy unveils hot polaron photoconductivity dynamics in metal-halide perovskites, J. Phys. Chem. Lett. **12**, 8732 (2021).

[25] M. Sendner, P. K. Nayak, D. A. Egger, S. Beck, C. Müller, B. Epding, W. Kowalsky, L. Kronik, H. J. Snaith, A. Pucci, and R. Lovrinčić, Optical phonons in methylammonium lead halide perovskites and implications for charge transport, Mater. Horiz. **3**, 613 (2016).

[26] A. S. Mishchenko, L. Pollet, N. V. Prokof'ev, A. Kumar, D, L. Maslov., and N. Nagaosa, Polaron Mobility in the "Beyond Quaiparticles" Regime, Phys. Rev. Lett. **123**, 076601 (2019).

[27] J. Devreese, J. D. Sitter, and M. Goovaerts, Optical Absorption of Polarons in the Feynman-Hellwarth-Iddings-Platzman Approximation, Phys. Rev. B **5**, 2367 (1972).

[28] A. S. Mishchenko, N. V. Prokof'ev, A. Sakamoto, and B. V. Svistunov, Diagrammatic quantum Monte Carlo study of the Fröhlich polaron, Phys. Rev. B **62**, 6317 (2000).

[29] D. Sels, A treatise on Wigner distributions: From particles and polarons to fields, Ph.D. thesis, Universiteit Antwerpen, 2014.

[30] R. Feynman and F. Vernon, The theory of a general quantum system interacting with a linear dissipative system, Ann. Phys. **24**, 118 (1963).

[31] S. A. Hartnoll and A. P. Mackenzie, Colloquium Planckian dissipation in metals, Revi. Mod. Phys. **94**(4), 041002 (2022).

[32] G. DeFilippis, V. Cataudella, A. S. Mishchenko, C. A. Perroni, and J. T. Devreese, Validity of the Franck-Condon Principle in the Optical Spectroscopy: Optical Conductivity of the Fröhlich Polaron, Phys. Rev. Lett. **96**, 136405 (2006).

[33] X. Gonze and C. Lee, Dynamical matrices, born effective charges, dielectric permittivity tensors, and interatomic force constants from density-functional perturbation theory, Phys. Rev. B **55**, 10355 (1997).

[34] C. Verdi, First-principles Fröhlich electron-phonon coupling and polarons in oxides and polar semiconductors, Ph.D. thesis, University of Oxford, 2017.

[35] G. Verbist, F. M. Peeters, and J. T. Devreese, Extended stability region for large bipolarons through interaction with multiple phonon branches, Ferroelectrics **130**, 27 (1992).

[36] J. T. Devreese, S. N. Klimin, J. L. M. van Mechelen, and D. van der Marel, Many-body large polaron optical conductivity in $SrTi_{1-x}Nb_xO_3$, Phys. Rev. B **81**, 125119 (2010).

[37] F. Brivio, J. M. Frost, J. M. Skelton, A. J. Jackson, O. J. Weber, M. T. Weller, A. R. Goñi, A. M. A. Leguy, P. R. F. Barnes, and A. Walsh, Lattice dynamics and vibrational spectra of the orthorhombic, tetragonal, and cubic phases of methylammonium lead iodide, Phys. Rev. B **92**, 144308 (2015).

[38] B. Guzelturk, R. A. Belisle, M. D. Smith, K. Bruening, R. Prasanna, Y. Yuan, V. Gopalan, C. J. Tassone, H. I. Karunadasa, M. D. McGehee, and A. M. Lindenberg, Terahertz emission from hybrid perovskites driven by ultrafast charge separation and strong electron-phonon coupling, Adv. Mater. **30**, 1704737 (2018).

[39] R. P. Feynman, *Statistical Mechanics: A Set of Lectures (Frontiers in Physics)* (Addison-Wesley, Boston, 1972).

[40] T. D. Schultz, Slow electrons in polar crystals: Self-energy, mass, and mobility, Phys. Rev. **116**, 526 (1959).

[41] C. H. Mousatov and S. A. Hartnoll, On the planckian bound for heat diffusion in insulators, Nat. Phys. **16**, 579 (2020).

[42] D. Sels, Dynamic polaron response from variational imaginary time evolution, arXiv:1605.04998.

[43] T. Ichmoukhamedov and J. Tempere, General memory kernels and further corrections to the variational path integral approach for the Bogoliubov-Fröhlich hamiltonian, Phys. Rev. B **105**, 104304 (2022).

[44] L. P. Kadanoff, Boltzmann equation for polarons, Phys. Rev. **130**, 1364 (1963).

[45] F. M. Peeters and J. T. Devreese, The 3/2 kT problem in the low-temperature polaron mobility theories, Phys. Status Solidi B **115**, 539 (1983).

[46] V. LOS, On the theory of the conductivity of crystals, Theor. Math. Phys. **60**, 703 (1984).

[47] V. F. Los, Influence of initial correlations on evolution of a subsystem in a heat bath and polaron mobility, J. Stat. Phys. **168**, 857 (2017).

[48] V. F. Los, Evolution of a subsystem in a heat bath with no initial factorized state assumption, Phys. A (Amsterdam) **503**, 476 (2018).

[49] A. M. A. Leguy, A. R. Goñi, J. M. Frost, J. Skelton, F. Brivio, X. Rodríguez-Martínez, O. J. Weber, A. Pallipurath, M. I. Alonso, M. Campoy-Quiles, M. T. Weller, J. Nelson, A. Walsh, and P. R. F. Barnes, Dynamic disorder, phonon lifetimes, and the assignment of modes to the vibrational spectra of methylammonium lead halide perovskites, Phys. Chem. Chem. Phys. **18**, 27051 (2016).

[50] J. T. Marshall and L. R. Mills, Second-order correction to Feynman's path-integral calculation of the polaron self-energy, Phys. Rev. B **2**, 3143 (1970).

[51] Y. Lu and R. Rosenfelder, Second-order correction to Feynman's path-integral calculation of the polaron effective mass, Phys. Rev. B **46**, 5211 (1992).

[52] M. Houtput and J. Tempere, Beyond the fröhlich hamiltonian: Path-integral treatment of large polarons in anharmonic solids, Phys. Rev. B **103**, 184306 (2021).

[53] K. K. Thornber and R. P. Feynman, Velocity acquired by an electron in a finite electric field in a polar crystal, Phys. Rev. B **1**, 4099 (1970).

[54] N. Janssen and W. Zwerger, Nonlinear transport of polarons, Phys. Rev. B **52**, 9406 (1995).

[55] J. Bezanson, A. Edelman, S. Karpinski, and V. B. Shah, Julia: A fresh approach to numerical computing, SIAM Rev. **59**, 65 (2017).

[56] J. M. Frost and B. Martin, https://github.com/jarvist/PolaronMobility.jl.

[57] M. Harvey, Imperial college research computing service (2017).